

AD-781 756

PRELIMINARY CREEP DEFLECTION DESIGN  
METHOD OF RADIATIVE METALLIC HEAT  
SHIELDS FOR ADVANCED AF VEHICLES

Werner R. Jansen

Air Force Flight Dynamics Laboratory  
Wright-Patterson Air Force Base, Ohio

December 1973

DISTRIBUTED BY:

**NTIS**

National Technical Information Service  
U. S. DEPARTMENT OF COMMERCE  
5285 Port Royal Road, Springfield Va. 22151

AD-781756

## DOCUMENT CONTROL DATA - R &amp; D

(Security classification of title, body of abstract and indexing annotation must be entered when the overall report is classified)

1. ORIGINATING ACTIVITY (Corporate author) AF Flight Dynamics Laboratory Advanced Structures Branch (FBR)		2a. REPORT SECURITY CLASSIFICATION UNCLASSIFIED	
		2b. GROUP	
3. REPORT TITLE  Preliminary Creep Deflection Design Method of Radiative Metallic Heat Shields for Advanced AF Vehicles			
4. DESCRIPTIVE NOTES (Type of report and inclusive dates) Final Technical Memorandum Report			
5. AUTHOR(S) (First name, middle initial, last name)  Werner R. Jansen			
6. REPORT DATE December 1973		7a. TOTAL NO. OF PAGES 72	7b. NO. OF REFS 43
8a. CONTRACT OR GRANT NO.  A. PROJECT NO. 13680101		9a. ORIGINATOR'S REPORT NUMBER(S)  AFFDL-TM-73-161-FBS	
C.  d.		9b. OTHER REPORT NO(S) (Any other numbers that may be assigned this report)	
10. DISTRIBUTION STATEMENT  Approved for public release; Distribution unlimited			
11. SUPPLEMENTARY NOTES		12. SPONSORING MILITARY ACTIVITY AF Flight Dynamics Laboratory AF Systems Command Wright-Patterson AFB, Ohio 45433	
13. ABSTRACT <p>In support of their eventual AF development and use, an analytical investigation of the relative structural efficiency of radiative, coated and uncoated metallic heat shields for long life operation was conducted. The parameters required to establish qualitative performance characteristics for design of reusable heat shields were determined. An optimum weight prediction method was proposed based on the criterion of allowable aero-limit deflection as a direct effect of cyclic creep elongation of the material.</p> <p>Requirements at various temperature exposures were checked against the potential of existing different high temperature alloys on both a strength-to-weight and stiffness-to-weight competitive basis. The feasibility of the mathematical model developed for creep deflection evaluation of different heat shield configurations was partly proven by comparing estimated results and published test data of structural performance. Some existing design capabilities were found inadequate or incomplete, as previous estimated TPS unit weights vary up to 100%.</p> <p>This is a unique analysis model and a great step towards consideration of all the important heat shield design parameters within one method for performance rating of existing and future necessary designs.</p>			

12

## KEY WORDS

## LINK A

## LINK B

## LINK C

ROLE

WT

ROLE

WT

ROLE

WT

Creep Deflection  
Heat Shields  
Design Method

ia.

PRELIMINARY CREEP DEFLECTION DESIGN METHOD OF RADIATIVE  
METALLIC HEAT SHIELDS FOR ADVANCED AF VEHICLES

WERNER R. JANSEN

Technical Memorandum AFFDL TM-73-161-FBS

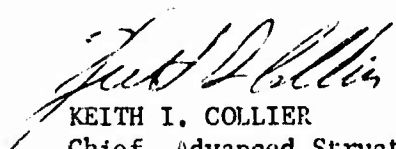
December 1973

Prepared under Project-Task-Work Unit 13680101

Air Force Flight Dynamics Laboratory  
Director of Laboratories  
Air Force Systems Command  
Wright-Patterson Air Force Base, Ohio

# PREFACE

This is a report of the work performed under Project/Task Area/ Work Unit 13680101 "Elevated Temperature Structural Concepts" in the Design Feasibility Group, Advanced Structures Branch, Structures Division, Flight Dynamics Laboratory. The work period covers investigations conducted in-house from September 1969 to June 1973. The manuscript of this report was released by the author for publication as a FBS Technical Memo.



KEITH I. COLLIER  
Chief, Advanced Structures Branch  
Structures Division

### ABSTRACT

In support of their eventual AF development and use, an analytical investigation of the relative structural efficiency of radiative, coated and uncoated metallic heat shields for long life operation was conducted. The parameters required to establish qualitative performance characteristics for design of reusable heat shields were determined. An optimum weight prediction method was proposed based on the criterion of allowable aero-limit deflection as a direct effect of cyclic creep elongation of the material.

Requirements at various temperature exposures were checked against the potential of existing different high temperature alloys on both a strength-to-weight and stiffness-to-weight competitive basis. The feasibility of the mathematical model developed for creep deflection evaluation of different heat shield configurations was partly proven by comparing estimated results and published test data of structural performance. Some existing design capabilities were found inadequate or incomplete, as previous estimated TPS unit weights vary up to 100%.

This is a unique analysis model and a great step towards consideration of all the important heat shield design parameters within one method for performance rating of existing and future necessary designs.

## Table of Contents

	<u>Page</u>
Preface	i
Abstract	ii
I. Introduction	1
1. Objective	1
2. History, Economical Importance	2
3. Design Philosophy	3
II. Design Criteria	3
1. Ground Rules	5
2. Approach	5
III. Method of Analysis	6
1. Design Parameters and Procedures	7
2. Creep Index Procedure and Results	8
3. Direct Method and Results	10
IV. Assessment of Materials Available for TPS Applications	14
1. TPS Design with Aluminum Alloys	15
2. Beryllium in TPS Design	16
3. Titanium Alloys	17
4. Superalloys and DSM	18
Nickel-base Alloys	19
Iron-base Superalloys and Stainless Steels	22
Cobalt-base Alloys	23
5. Refractory Alloys in TPS Design	24
Columbium Alloys	24
Tantalum Alloys	27
V. Conclusions/Recommendations	28
References	30
Figures	33
Tables	48
Appendix	54

### List of Illustrations

<u>Fig.</u>	<u>Title</u>	<u>Page</u>
1	Effect of multiple re-entry on creep [8] .	33
2	Load-temperature profile.	33
3	Typical heat shield with support structure.	34
4	Parameters for heat shield design.	34
5	Application-fixed algorithm "1".	35
6	Constant creep condition and deflection criterion at different attachments.	36
7	Constant creep condition and attachments at different deflection criteria.	37
8	Constant deflection criterion and attachments at different creep conditions.	38
9	Quasi-elastic case at low creep index.	39
10	Materials concepts and assessment algorithm "2".	40
11	Creep-index trade-off.	41
12	Newton's interpolation.	41
13	Square channel cross section.	42
14	Net panel weights at different temperatures (fixed panel depth).	42
15	Net and support weights vs. panel length.	43
16	Variational trends of properties at constant panel depth.	44



# List of Illustrations

(Cont.)

<u>Fig.</u>	<u>Title</u>	<u>Page</u>
17	Variational trends of properties at constant creep and stress level.	45
18	Weight vs. panel length, comparison of constant stress and creep at con- stant panel depth.	46
19	Comparison of TPS weights.	47

### List of Tables

<u>Tab.</u>	<u>Title</u>	<u>Page</u>
1	Adiabatic wall and stagnation temperature.	48
2	Elastic boundary constants.	48
3	Criteria of total deflection.	48
4	Creep data for 2219-T87 aluminum [12].	49
5	Creep strength (.2%) of titanium alloys.	49
6	Creep data for Ti-6-4 (STA) [12].	50
7	Metallic heat shield weights at temperature [5].	50
8	Cyclic creep of super alloys [8].	51
9	Maximum temperatures for separate stress cyclic and temperature cyclic prediction [14].	52
10	Minimum gages for L-605 (McDonnell).	52
11	Design data for L-605 heat shield [7].	52
12	Performance of oxidation protective tantalum alloy coatings.	53
13	Weight penalties of coated T-222 TPS designed for creep [15].	53

## Nomenclature

$c, c(G)$	creep strain of outer fiber
$const_1, const_2$	constants of stress function
$c_1, c_2, c_3$	constants
$EI \text{ [}\# \cdot \text{in}^2\text{]}$	bending stiffness
$F(G), F_0, F'_0$	function of stress
$f, f_{\text{plastic}}, f_{\text{elastic}} \text{ [in.]}$	mid span deflection
$g \text{ [in.]}$	gage thickness
$I \text{ [in}^4\text{]}$	cross sectional moment of inertia
$L \text{ (or } l) \text{ [ft]}$	panel length
$M \text{ [}\# \cdot \text{in}\text{]}$	bending moment
$P, P_{\text{surface}} \text{ [psi, psf]}$	panel pressure
$S \text{ [}\#/\text{ft}\text{]}$	averaged support weight
$T, T_{\text{surface}} \text{ [}^\circ\text{F}\text{]}$	temperature
$t \text{ [in.]}$	panel thickness
$W, W_{\text{total}} \text{ [}\#/\text{sqft}\text{]}$	unit weight of square channel section
$x, y \text{ [in.]}$	cross sectional coordinates
$\epsilon$	elastic strain of outer fiber
$\epsilon_{\text{total}}$	total allowable strain
$\epsilon_0 \text{ [in}^{-1}\text{]}$	elastic unit strain
$\rho \text{ [}\#/\text{sec}^2/\text{in}^4\text{]}$	mass density of material
$\sigma \text{ [ksi, psi]}$	stress level at outer fiber
*	symbol for multiplication

## I Introduction

Increased operational speeds, essential for superior military aerospace vehicles, cause aerodynamic heating of the airframe. This phenomenon is usually explained in a way, that the velocity of the air flowing around the vehicle is reduced to zero at the vehicle surface, and the kinetic energy of the air stream which enters the boundary layer must appear as heat. Temperatures,  $T$ , are the adiabatic wall temperature,  $T_a$ , or the stagnation temperature,  $T_s$ , depending on the type of recovery factor,  $R$  [Eq.1, Tab.1].

$$T = T_{\infty} \left( 1 + R \left( \frac{\gamma - 1}{2} \right) M_{\infty}^2 \right) \quad (^{\circ}R) \quad [\text{Eq.1}]$$

$T = T_a$  = adiabatic wall temperature for

Prandtl recovery factor,  $R = .864$

$T = T_s$  = stagnation temp. for  $R = 1$ .

$T_{\infty}$  = ambient air temp.

(395  $^{\circ}R$  at 75,000 ft, 435  $^{\circ}R$  at 120,000 ft)

$\gamma = 1.4$

$M_{\infty}$  = Mach number

Local aerodynamic pressure acting on the surface of the vehicle is a fraction of the free stream dynamic pressure,

$$P_{\text{surface}} = .5 * \gamma * p_{\infty} * M_{\infty}^2. \quad [\text{Eq.2}]$$

The typical operation of a vehicle at hypersonic atmospheric flight consists of (1) high altitude, 100,000 to 250,000 ft, temperature critical flight condition at speeds of 10,000 to 30,000 ft/sec with moderate dynamic pressures of below 1 psi (144 psf). Temperatures generated adversely influence the load carrying capability of the airframes involved. Shielding the structure is feasible thru different thermal protection systems (TPS). (2) The flight condition at lower altitudes and velocities experiences pressures of several psi at moderate temperatures.

### 1. Objective

In support of their eventual AF development and use, this work effort is (1) to conduct an analytical investigation of the relative structural efficiency of radiative metallic heat shields for long life operation, (2)

to prove the feasibility of the mathematical model developed for creep deformation evaluation of different heat shield configurations by comparing estimated results and actual test data of related efforts to optimize for minimum weight, and (3) to determine beneficial applications of existing materials to suit environmental conditions.

## 2. History, Economical Importance

A literature search in 1969 [2] revealed that ablative, one-flight heat shield technology using fiber reinforced organic materials was fairly well developed, while limited information only was available on metallic reusable, structurally stable surface panels to meet 800 thru 1600°F thermal requirements of atmospheric flight conditions. Elongation due to creep of these radiative heat shields proved to override other strength requirements [3]. Today, a major technical goal for NASA still is the development of heat shields reusable for one hundred shuttle orbiter and space plane re-entry cycles [4]. The economic importance of this becomes evident [5] upon considering pound reduction/increase in dry weight directly related to unit weight change in the thermal protection system (TPS) on the wetted area. This weight reduction/increase is totally equivalent to gained/lost payload, that can be of the order of 10,000# for an orbiter of 20,000 ft<sup>2</sup> wetted area experiencing a .5#/ft<sup>2</sup> change in TPS.

Some ground rules were selected as TPS design criteria in 1967 [6]. Materials were projected to be of the 1970 state-of-the-art. External heat shield structures were planned to have a reuse life of five (5) cycles or greater, except where conditions warrant otherwise. The panels designed for ease of replacement, had to be capable of transferring external normal pressure loading into the primary shell structure. Critical loads were discovered to occur at room temperature during ground handling operations of the shuttle. Weight savings were found to depend primarily on minimum gage fabrication capability of .005" or less. These thin gages are feasible due to the very low loads experienced during high altitude flight. The limit design static analysis employed a safety factor of 1.4 to .2% of yield off-set. This type of approach taken due to lack of confidence in the analytical method over many years, usually worked satisfactory in conventional aircraft design. Creep investigations were not extensively performed by the originators of these criteria to find that plastic deformation dominates the TPS design.

Several design studies for shuttle vehicles exist. There are typical requirements for long range and short cross range missions (7), both laid out for a hundred flights. Design loads are presented in realistic time-temperature, time-pressure profiles for representative locations at the external vehicle surfaces, with higher temperatures and pressures usually occurring during the longer missions.

### 3. Design Philosophy

An optimized panel can be expected to experience in the most critical descent phase critical strength or critical deflection conditions at one time at least, or the conditions at two different instances. Therefore, the panel should be designed for strength and stiffness, what would be an adequate design philosophy without the thermal creep phenomenon [7]. "Light weight" TPS design, however, necessitates careful observation of the detrimental plastic strain in relationship with elevated temperature, exponential in nature, dominating over elastic stiffness behavior. Long time cycling of load and temperature, as a matter of fact, has been found to deteriorate some superalloys such that the creep rate is up to 10 times greater [8] than continuous constant conditions [Fig. 1]. Severe changes in temperature and stress will affect composition or phase in a material, which may differ in inner and outer layers, and thereby induce stresses causing accelerated creep. Only original cyclic re-use data should be used for design purposes. Conversion of existing steady-state data by some means of correction factor is of questionable validity.

### II Design Criteria

Heat shield design criteria are to be established based on realistic test data to size the panel structure for both strength and elastic/plastic deflection requirements.

Temperature-pressure combinations considered are those occurring in the operational flight regime of hypersonic flight and re-entry [Fig. 2]. These combinations for the critical locations of a typical shuttle vehicle, 160' long, initially at an atmospheric altitude of 400,000 ft, have been described [7] over a period of 3600 sec. The data indicate that temperature increases within 250 sec. to 1950 deg F at the most critical station during the long cross range reentry. Temperatures are in the range of 1,020 and 1,950 deg F at the bottom centerline for 2,550 sec. Pressures will occur not higher than .35 psi for both long and short range reentry conditions. Maximum temperature for short range reentry is 1,530 deg F only after 300 sec. NASA space shuttle orbiter heat shields [4] have to withstand 3 psi air pressure during boost at which time panels are at 70°F. During reentry, maximum pressure across the panels is .2 psi or about 7% of R.T. load. Pressures are of high magnitude for modulated re-entry flight, of importance for AF vehicles operating in these flight regimes, at accelerated and presumably higher aerodynamic loads.

Panel deflection results in turbulent flow and excessive heating [4]. NAR reported maximum deflections on their heat shields to occur due to thermal gradients in the first 5 minutes of re-entry. Overheating of panels with surface waviness in hypersonic flow has been demonstrated [6] to be the principle reason of different heat shield failures, such as sudden oxidation, burn-up, or a mixture thereof. Quasi-static panel creep due to one cycle or more of bending, caused by the transverse air pressure,

accumulates permanent surface deformation. Therefore, a dominating design criterion is that heat shields maintain their shape within tolerable limits.

The surface waviness investigation [6] for the critical heating condition on a low L/D lifting body indicates allowable deflections of .25 to .5 in. before heating rates significantly higher than those of an undeflected surface occur. Aerodynamic cleanliness at aftward locations was found less critical. These results are similar for all lifting spacecrafts. In addition, height-over-thermal boundary layer thickness has been investigated, including laminar and turbulent flow at small angles of attack as a function of the undisturbed heating rate, in order to minimize aerodynamic drag due to sine wave protrusion. The increase in heating was found not to be strongly dependent on panel length for the range of test data shown.

The permissible total TPS panel deflection used in this study is at a critical forward location, expressed as one tenth of an inch plus one hundredth of the unsupported panel length in the direction of the air stream. Another version of allowable deflection, two hundredth of panel length, was accepted for comparison. These two criteria are identical at a panel length of 10. inch. Total deflection is made up of elastic and plastic deflection.

A few remaining points of design interest concern the integration of the heat shield with intermediate insulation, attachment system or entire vehicle. The optimized thin gage heat shield structurally interferes with the backup insulation and their support to the substructure, and is characterized by different performance characteristics, not only temperature-load endurance and minimum weight, but reliability, inspection and refurbishment possibility, and the important different elements of cost. Analysis of candidate backup-insulations, when considered, should include mechanical (acoustic noise) and thermal evaluation. Fastening and joining create structural restraining due to thermo-stresses and there is another problem [4]: mechanical fasteners for high temperature use are limited to rather low stresses due to relaxation under load. A decision, not under the scope of this program, concerns a system's oriented optimum panel thickness. Thicker heat shields, usually lighter per unit surface, cause extra volume of "dead space" and are less advantageous for flight performance. The most severe temperature/pressure environment obviously exists at the stagnation point of the leading edge, a rounded panel which principally behaves like a flat panel accounting for the influence of geometric curvature. Inspection after each flight and replacement of the individual heat shield, which failed too early, could justify substitution of a lower factor of safety for that one relayed on in accordance with better TPS performance.

Heat shield technology for NASA and AF vehicles is somewhat similar. Loads on heat shields of advanced military space and shuttle vehicles under service and environmental conditions would be more severe than those for NASA vehicles. The greater number of flights for AF vehicles may be a more severe mission requirement.

## 1. Ground Rules

Hot radiative metallic heat shield concept [Fig. 3] is one of four different approaches under study to various degrees by NASA and potential contractors. The others are: hot structures, ceramic insulative heat shields, and ablative heat shields [4].

In the concept of hot structures, the entire heat load and structural load is taken by the structure itself. A pioneering example is the AF hypersonic glide re-entry vehicle, ASSET, built of heavy super- and refractory materials by McDonnell and flight tested in 1963. Moderately hot structures are the supersonic airplanes flying, built of aluminum and titanium.

The radiative metallic heat shield takes no primary structural loads, but sees aerodynamic pressure loads and transmits these to the structure [4]. Critical areas are associated with (a) high temperature material behavior including creep elongation causing excessive deflection and rate of oxidation, (b) performances relative to thermal expansion buckling and flutter, (c) minimum gage handling and fastening fabricability, and (d) maintenance inspection and field repair.

Materials for heat shield application have to be metallurgically stable and strong enough to carry all the loads of the thermal environment. Desirable properties are high strengths, high elastic moduli, low creep values, and small densities. The following basic problems are common in all heated structures. Strength and stiffness of structural materials due to the load-temperature environment decrease and creep action takes place through the load-temperature-time exposure resulting in accumulation of permanent deformation. Use of the materials is usually limited to a maximum temperature, roughly half way between room temperature and melting point for conventional and much higher for advanced metallic systems. Creep properties are different in longitudinal and transverse direction of sheet for most of the engineering metals, due to material processing. Creep data below ultimate levels of stress rupture for constant conditions have been identified for beryllium, titanium alloys, steel, nickel-and cobalt-base alloys and dispersion strengthened metal systems (DSM), and a few refractory metals. These conventional steady-state data come mostly from handbooks and literature [9,10]. Less frequent cyclic data, accounting for synergistic effects of both temperature and load cycling, more realistic for reusable heat shields, were generated under recent NASA space shuttle or SST programs [8,11,12].

## 2. Approach

Pioneer work [13] in 1932 on a lead beam under a uniform bending moment tested at room temperature revealed that (a) plane sections remain plane during



creep, (b) redistribution of stresses occurred relatively quickly, and (c) creep deformation of the beam could be calculated from simple creep data. It was possible to conduct a similar analysis [15] suiting the experiment on a coated tantalum beam with non-uniform bending moment distribution at high temperature. Therefore, the heat shield structure was one-dimensionally idealized as a beam [Fig. 1] under pure pressure bending with no structural or thermal inplane stresses superposed. This is technically feasible for concepts with no longitudinal and lateral constraints, such as interferences with substructure and insulation. Averaged area loading during the time interval chosen, from characteristic trajectory profiles at representative body stations, are the pressure differential between the outside and inside of vehicle and other loads in transverse direction on the panel. Two further idealizations were assumed. Shear stresses obtained by the standard elastic formula are non-critical, as peak values attained in the panel sections are too low to be indicative of design allowables. Temperature profiles averaged over panel area reflect the realistic thermal situation of conduction and radiation. Assumption of uniform heating eliminates the problems of differential expansion such as thermal buckling.

More refined creep deflection analysis has been used in a related effort [15] to come up with creep strains taken from creep data according to the stress levels at six (or an arbitrary number of) locations, distributed over half the panel length. This distribution of unit creep strain (or curvature), integrated twice with necessary constants of integration as determined from boundary conditions, determined the maximum plastic beam deflections. The greater numerical effort of the approach [15] is not necessary for this preliminary prediction which is even more on the conservative side.

### III Method of Analysis

The method of analysis applied was general, non-system-oriented, and used material/structural data applicable to heat shields and realistic flight conditions as the variable input. Panel loading was restricted to averaged lateral pressures. Several heating/loading cycles were combined to one computational cycle, to summarize the entire time from successive flights at constant load and temperature, however, considering the detrimental effects of the multi-flight environment. The non-load bearing concept with air loads only was used to avoid the thermal expansion problem. Bending of the basic structural beam element was analyzed rather than the two-dimensional plate. The method of determining beam deflection from creep data was to obtain the strain and convert it into an apparent bending moment at each station after exposure to temperature and time under operating loads. The variety of different heat shield mountings was realized by incorporating the

free-free (FF), free-clamped (FC), and clamped-clamped (CC) cases of end attachment into the beam equations.

Other assumptions made to simplify the analysis are discussed below. A cross-sectional bending moment symmetrical about the plane perpendicular to the panel in longitudinal direction was assumed causing elastic and plastic deformation to contribute to the total heat shield deflection. Stretching was not considered, as the strain at the location of the neutral axis was assumed to remain zero. Plane cross sections before bending were assumed to remain plane after bending, and the strain at a point in a given cross section varies linearly with its distance from the neutral axis. This yields a conservative estimate of creep deformation leading to a simplified analysis across the cross section and along the beam that considers the special case of linear creep behavior with strain rate proportional to stress. The stress distribution consequently agrees with the linear elastic case, and the neutral axis for creep and elastic deformation both stay the same, as well as the fictitious plastic moment of inertia at any place along the beam of constant cross section equals moment of inertia. Another simplification was to interchange the actual creep on the compression side of the heat shield, usually not available in data format, for steady-state secondary creep at given stress levels in tension.

Necessary calculations were performed by means of computer routines in FORTRAN, based on the analysis method developed. Evaluated results as processed by the CDC 6600 computer system are selectively reported. Instead of elaborating at this place on the description of computer routines used, the reader familiar with FORTRAN may consult the Appendix.

### 1. Design Parameters and Procedures

There are sixteen (16) important interrelated design parameters, consideration of which is essential for effective radiative heat shield design. These are application (temperature, pressure load, aero limit deflection), configuration (end fixity, panel depth, bending strength, bending stiffness, cross section), material (gage thickness, creep stress level, creep rate, modulus of elasticity, material density), and panel comparison (weight per unit area, size, life) [Fig. 4].

Two different design procedures basically containing the inter-relationship of these parameters were developed. One procedure was to match results from two algorithms (see section 2) namely "creep index" charts ("1") and tabulated material data ("2"). The definition of creep index, found to be a practical parameter to use within this procedure, is creep (%) divided by height of panel (in.). The second direct method developed combines the two separate algorithms of the first procedure, and was used for advantages explained in the following section.

## 2. Creep Index Procedure and Results

Algorithm "1" [Fig. 5] of the creep index procedure, an elastic-plastic and material independent deflection criterion, calculates and plots zero-margin-deflection curves of constant bending strength and constant bending stiffness from smallest values applicable in increments of 200%, 500%, 1000% etc. to cover a wide range of parametric design interest for panel sizes of .5 to 5 feet, and for pressure loads of .5 to 5. psi, at the predetermined total maximum deflections of the two deflection allowables previously indicated. For each individual chart, the creep index is a constant, which of course is a function of the creep environment. In addition, each of the three types of attachments makes a different chart. The range of creep indices, technically feasible for heat shields, may vary from .0000025 to .05 ( $\text{in}^{-1}$ ). Different charts [Figs. 6, 7, 8, 9] of algorithm "1" explain the influence of creep condition, deflection criterion, and attachment condition as design functions. The changes of curves of constant bending moment,  $M$  (continuous lines), and those of constant stiffness,  $EI$  (dashed lines), shall be discussed for constant creep condition and deflection criterion held constant at different attachments [Fig. 6], for constant creep condition and attachments at different deflection criteria [Fig. 7], and constant deflection criterion and attachments at different creep conditions [Fig. 8].

a. The results are lines of constant bending moment ( $M$ -curves) being fairly insensitive to changes of the two deflection criteria and percentages thereof (in [Fig. 7] they proceed from deflection criterion "one" into "two").  $M$ -curves stay identical for different creep conditions too [Fig. 8]. They move towards larger panel lengths for stiffer edge conditions [Fig. 6] (see lines  $M=100$ ).

b. Lines of constant stiffness ( $EI$ ) move toward larger panel lengths for increasing attachment stiffness [Fig. 6] and percentage of deflection allowable [Fig. 7], and for decreasing creep indices [Fig. 8], i.e. they intersect with the curves of constant bending strength (in fairly fixed positions) at larger panel lengths, however, at lower pressure loads.

c. The most efficient design (not shown in the charts) is under clamped-clamped condition at 100% of the second assumption made for allowable deflection, in short notation: CC2-100% [pgs. 4,7].

d. Pressure load vs. panel length ( $p-l$ ) diagrams, comparable at the same type of boundary conditions, are almost identical for small creep indices. In these cases creep does not constitute a major deflection problem [Fig. 9]. Charts drastically change at larger creep indices. A quasi-elastic example case at the low creep index of .0000025  $\text{in}^{-1}$ , condition FF-100%, was evaluated and matched with the curves [Fig. 9]. In other words, for large panel lengths and at small creep indices (low plasticity), small panel stiffnesses only are required. Larger stiffnesses are

necessary for panels with attachment conditions more flexible, to create similar optimum lengths and loading conditions.

e. A phenomenon was found that could be called "creep barrier" for bending stiffnesses, EI, approaching very large values, in which case maximum panel sizes are reached and contribution of elastic deflection to the total allowable deflection is negligible [Fig. 6, 7, 8].

f. The interchangeability of algorithm "1" working charts shall be indicated within the same category of attachment condition and type of deflection criterion. Higher deflection allowables and creep rates together balance lower quantities respectively, i.e. charts are interchangeable for ratios of creep index-to-percentage of deflection being constant. For example, the chart of one hundred percent of creep deflection,  $.1" + .01L$ , free-free support at a creep index of .0025 (2nd plot of [Fig. 8]) is identical with the chart of fifty percent of that creep deflection at an index of  $.00125 (\text{in.}^{-1})$ .

Algorithm "2", a material concepts and assessment routine [Fig. 10], tabulates cross sectional properties, data of bending strength (M), bending stiffness (EI) and normalized panel weight for up to seven (7) different panel concepts with geometrical dimensions as the variable input: beaded, hat, sandwich, rib, u-core, vee-corrugation, and zee-stiffened. Practical designs usually fall into these categories. Data listings are in rising orders for screening purposes. Specific bending strengths and stiffnesses, however, were found to scatter slightly for series of configurations considered.

The selective combination of algorithm "2" with the application fixed algorithm "1", as indicated above, complements the first design procedure. Selection of the cross section of required bending strength at the highest strength-to-weight ratio possible, along with the required bending stiffness at the highest stiffness-to-weight ratio possible presents a two-fold optimization problem. Strength and stiffness have to be at a distinct ratio for optimal low panel weight at a desired condition of panel length and pressure load. Comparing one design with the other is obviously rational only for constant temperature and time endurance. This led to the exploration of several analysis approaches of which (1) creep-index trade-off at constant weight thru modification of stress-level, gage thickness and panel depth, (2) modification of allowable total deflection and (3) switch within available material systems principally contain the basic features.

To study a panel of one material system (at constant temperature endurance) could be called stress level modification trade-off. An increase (decrease) of the operating stress level causes higher (lower) creep within the cross section. Consider a requirement to optimize a

panel for creep indices .0005, .001, .0025, and .005 ( $\text{in}^{-1}$ ), with bending moments of 70, 80, 90, and 100 ( $\text{lb-in}$ ) respectively, all at bending stiffness of 6000 ( $\text{lb-in}^2$ ). These data combinations were actually picked from an algorithm "2" material table, all at the same unit weight. With the curves of constant bending moment fairly unchanged in the four design charts (CC1-100%) of creep indices indicated, the curves of stiffness ( $6000 \text{ lb-in}^2$ ) move to 1.2 ft shorter panels, from the smallest creep index to the highest one, however, gaining an allowable load increase of 2.7 psi. A curve of constant weight could be drawn in the p-l plane to connect the intersections of appropriate strength and stiffness curves [Fig. 11], unbroken and dashed lines respectively. The theoretical upper limit on this curve is represented by the bending strength at creep rupture, the limit on the other side by the technically achievable highest stiffness value at the lowest creep rate possible. This analysis approach (1) can be comparatively used in different material systems, approach (3).

Changes of the allowable deflections, approach (2), of the panel with cross sections fixed is justified only under the scope of vehicle performance evaluation. Change to a deflection allowable smaller (greater) than originally assumed, causes panel lengths to decrease (increase) and load carrying capability to go up (down).

Analysis approaches (1 thru 3) presented so far may be seen as point designs, because of no effort undertaken to operate with applied stress as a function of creep (at constant temperature and time). This relationship became part of the second design procedure developed, using in addition the equations of this procedure.

### 3. Direct Method and Results

Total allowable deflection based on deflection criterion equals elastic deflection plus plastic deflection, or: total allowable strain equals elastic strain plus plastic strain.

Definition for elastic unit strain is:

$$\epsilon_o [\text{in}^{-1}] = \frac{\text{bending moment, } M \text{ #-in}}{\text{bending stiffness, } EI \text{ #-in}^2} \quad [\text{Eq. 3}]$$

Elastic strain of outer fiber is:

$$\epsilon [\text{in/in}] = \frac{M}{EI} * \frac{1}{2} \text{ panel thickness } (t) = \epsilon_o * \frac{1}{2} t \quad [\text{Eq. 4}]$$

$$\text{Hooke's law in terms of unit strain is } \sigma = \epsilon * E = \frac{1}{2} t * \epsilon_o * E \quad [\text{Eq. 5}]$$

with stress level,  $\sigma$  [ksi, psi] at the outer fiber causing creep strain,  $c$  [%, in./in.], which is material, temperature and time dependent. Youngs modulus,  $E$  [psi] is material and temperature dependent.

The temperature, T, and the local aerodynamic pressure,  $p = p_{\text{surface}}$ , generated adjacent to the structure [Eqs. 1 and 2] depend on the operational environment.

The required bending moment for strength, depending on type of end fixity,  $c_1$ , is  $M = c_1 * \text{pressure load} * \text{length}^2$  [#-in] [Eq. 6]  
for a 1 inch wide section.

Elastic deflection is:

$$f_{\text{elastic}} [\text{in.}] = c_3 * \text{pressure load} * \text{length}^4 / \text{bending stiffness} \quad [\text{Eq. 7}]$$

$$f_{\text{elastic}} = \frac{c_3}{c_1} \frac{M}{EI} L^2 = \frac{c_3}{c_1} \epsilon_b L^2 = 2 * \frac{c_3}{c_1} * \frac{\epsilon L^2}{t} = c_2 * \frac{\sigma L^2}{Et}$$

$$c_2 = \frac{2 * c_3}{c_1} \quad [\text{Tab. 2}]$$

Assuming the plastic strain-deflection relationship in correspondence with the elastic one, the elastic strain,  $\epsilon$ , is replaced in [Eq. 7] by the plastic strain to find the plastic deflection,

$$f_{\text{plastic}} = c_2 * \frac{\sigma L^2}{t} \quad [\text{Eq. 8}]$$

Total allowable deflection is:  $f_{\text{total}} = f_{\text{elastic}} + f_{\text{plastic}}$  [Eq. 9]

$$f_{\text{total}} = c_2 * \frac{\text{length}^2}{\text{thickness}} * \left( \frac{\sigma_{\text{outer fiber}}}{E} + \text{creep strain} \right) [\text{in.}]$$

Deflection criteria are contained in [Tab. 3].

The total allowable strain is:

$$\epsilon_{\text{total}} = \text{total deflection} * \text{thickness of panel} / c_2 * \text{length}^2 [\text{in./in.}] \quad [\text{Eq. 10}]$$

$$\text{The function of } \sigma, F(\sigma) = \frac{\sigma_{\text{outer fiber}}}{E} + c(\sigma) - \epsilon_{\text{total}} = 0 \quad [\text{Eq. 11}]$$

must be solved.

An example for using the creep equation of solution-treated and aged Ti-6Al-4V alloy sheet [8] is presented.

Equation for creep strain, percent:

$$(1. \% = .01 \text{ in./in.})$$

$$c = e^{.00225 - \frac{2758}{T-917}} * \text{stress}^{.0159 + \frac{105.8}{T-975}} * \text{time}^{-.924 - \frac{3.759}{T-1047}} \quad [\text{Eq. 12}]$$

T=Fahrenheit+460.

Approx. range for validity of [Eq. 12]:

temp.=600. thru 800. °F; stress=6. thru 110. ksi;

time=1. thru 500 hrs.; creep=.00001 thru .015 in./in.

Newton's interpolation formula was used to solve [Eq. 11], as shown in [Fig. 11]: Find  $\sigma = \sigma_{\text{outer fiber}}$  at  $F(\sigma)=0$  in

$$F(\sigma) = \text{const}_1 * \sigma^{\text{const}_2} + \frac{\sigma}{E} - \epsilon_{\text{total}} \quad [\text{Eq. 13}]$$

Iterative procedures as follows, with the first step:

$\sigma_0 = \epsilon_{\text{total}} * E$ . Then:

$$F_0 = \text{const}_1 * \sigma_0^{\text{const}_2} + \frac{\sigma_0}{E} - \epsilon_{\text{total}} \quad \text{and}$$

$$F'_0 = \text{const}_1 * \text{const}_2 * \sigma_0^{\text{const}_2-1} + \frac{1}{E} ;$$

$$\sigma_1 = \sigma_0 - \frac{F_0}{F'_0} . \quad [\text{Eq. 14}]$$

Finally, the repeatative step using [Eq. 13] and [Eq. 14] such as  $F_0 \rightarrow 0$ .

Creep law [Eq. 12] as used in the iteration:

$$\text{creep strain (in./in.)} = \text{const}_1 * \sigma^{\text{const}_2} = c(\sigma) \quad [\text{Eq. 15}]$$

$$\text{const}_1 = .01 * e^{.00225 - \frac{2758}{T-917}} * \text{time} e^{-.924 - \frac{3.759}{T-1047}} .$$

$$\text{const}_2 = e^{.0159 + \frac{105.8}{T-975}} .$$

Moment of inertia is for a 1 inch wide section:

$$I (\text{in.}^4) = \text{bending moment} * \text{panel thickness}/2. * \text{stress} \quad [\text{Eq. 16}]$$

$$I = .0005 * M * t/\sigma (\text{ksi})$$

The square channel cross section [Fig. 13] was chosen to represent other technically feasible cross sections for the reason indicated [pg. 9]:

$$I = \int_{-\frac{t}{2}}^{+\frac{t}{2}} xy^2 dy \quad [\text{Eq. 17}]$$

$$\text{Per unit width: } I = \frac{gt^2}{12} + \frac{gt^2}{2} = 1.714 * gt^2 \quad [\text{in}^3]$$

Gage thickness of square channel cross section,

$$g = 1.714 * I/t^2 \quad [\text{in.}] \quad [\text{Eq. 18}]$$

is the only value required in this case to calculate cross sectional I.

Weight per square inch:

$$W = 3. * g * g \quad \text{and}$$

$$W (\#/sqft) = 432. * g * g \quad [\text{Eq. 19}]$$

Normalized panel weight with averaged support weight, S (#/ft), is

$$W_{\text{total}} = W + \frac{S}{L} \quad [\text{Eq. 20}]$$

The weight penalty of the overall TPS due to necessary attachment fixtures,  $W_{\text{total}}$ , increases for every additional mounting station, and decreases for larger panel sizes with less attachments, however, at the cost of heavier weight per square foot of panel area. To this extent, a trade-off optimization of weight is achievable.

The qualitative content of Eqs. 3-20 is reflected in Figs. 14-18. Normalized panel weights, net and with supports, as a direct numerical result of parametric variation of lateral pressure load in increments of .2 psi and of panel length in increments of .5 ft were derived for 600, 700 and 800°F, and 500 hours exposure, using a stress-creep relationship for Ti-6-4 sheet [9] in a constant-depth-variable-stress approach [Fig. 14]. Data are for a .75" square cross sectional geometry at a .6 psi pressure differential. The boundary condition is arbitrarily chosen "fixed-clamped", as well as the deflection criterion of 2/100 of panel length. Line (B) marks an arbitrary minimum gage restriction of .5 mil, yielding a TPS weight of  $432 * .16 * .005 = .346 \text{ \#/ft}^2$  or higher.

Continuation of this study [Fig. 15], again for fixed panel thickness, i.e. floating stress and creep levels, presents net and support weights.

Line markings show:

- (0) net panel weight,
- (1) net plus support (.2 #/ft) weight,
- (A) pressure loads (.2, .4, .6 psi),
- (B) gage thickness (.005 in.),
- (C) stress level, 20 [ksi] and creep, .0031 [-], at length, 3 [ft].
- (D) stress level, 15 [ksi] and creep, .002 [-], at length, 4.5 [ft].

Variational trends of other pertinent parameters are compared vs. panel length for constant panel depth [Fig. 16] and constant creep/stress level [Fig. 17], respectively. Here again, the choice of the alloys, Ti-6Al-4V and Ti-7Al-12Zr, is arbitrary.



Scale interpretation [Fig. 16], value at 4.5 ft, and tendency:

(A) bending stiffness, 56,000. [#-in <sup>2</sup> ]	}	great increase
(B) bending strength, 200. [#-in]		
(C) gage, .017 [in.]		
(D) weight, 1.16 [#ft <sup>2</sup> ]		
(E) total deflection, 1.1 [in.]	}	moderate increase
(F) elastic deflection, .42 [in.]		
(G) panel depth, .75 [in.]	}	constant
(H) creep, .002 [-]	}	decrease
(I) stress level, 15. [ksi]		

Scale interpretation [Fig. 17], value at 4.5 [ft], and tendency:

(B) bending strength, 220. [#-in]	}	great increase
(A) bending stiffness, 150,000 [#-in <sup>2</sup> ]		
(E) total deflection, 1.1 [in.]	}	moderate increase
(D) weight, .73 [#ft <sup>2</sup> ]		
(F) elastic deflection, .18 [in.]		
(G) panel depth, 14 [in.]		
(C) gage, .01 [in.]	}	constant
(H) creep, .005 [-]		
(I) stress level, 13 [ksi]		

It is remarkable to note severe increase of gage and weight by designing with constant panel depth. Gage and weight increases are less for constant creep and stress level design, yielding better heat shield performance in the latter case. These facts are intentionally demonstrated [Fig. 18] for a parametric constant stress level range of 5.1 thru 7.2 [ksi], and a constant depth range of .75 to 1.5".

An important result demonstrated by this analysis, was that creep strain totaling close to 1%, as assumed operationally feasible [3], is fairly high.

VI Assessment of Materials Available for TPS Applications

Materials considered for application in "wetted" areas were noted [7] by temperatures ranges they are capable to experience without failure, separated

into below 800°F, 800, 1400, 1800, 2200, and over 2200°F. To determine the percentage of surfaces to fail within a certain range depends on the highly complex design configuration of a vehicle. The approximate maximum use temperatures for metallic TPS materials and the approximate percentages of vehicle areas below maximum use temperature are according to another orbiter study [11] for titanium 900 deg F (25-50%), superalloys 1830 (65-90), dispersion strengthened nickel chromium 2100 (85-95), coated columbium 2370 (90-98), and coated tantalum 2730 (95-98).

Of equal importance is the recognition of uncoated and coated metal systems of promising endurance strength and creep resistance that have been experimentally identified for application in the temperature range of below 800 thru 2200°F to meet requirements as dimensionally stable non-load bearing reusable surface panels [8, 11]. Data would have to be screened for stress levels causing up to one half per cent elongation due to plastic deformation over accumulated times of up to 50 hrs or over, equivalent to 100 load-temperature cycles or more under extreme space atmospheric conditions. Whenever possible, the synergistic influence of cycling as compared with steady state condition has to be assessed.

#### 1. TPS Design with Aluminum Alloys

To keep the primary aluminum structure of a delta-body orbiter for 1500 NM cross range at a 200°F upper temperature, Lockheed [16] studied on the windward surface area the comparative performance of active TPS, using flowing of water glycol through aluminum tubes attached to the interior surface, and passive TPS with 6#/ft<sup>3</sup> Dyna Flex insulation.

Airframes primarily built of aluminum are very cost effective and may serve, when sufficiently insulated from heat of re-entry, to pick up body bending, compression and shear of a space vehicle. The structure may extend to the external moderately hot surface at aft sections of the vehicle. In this case, the aluminum skin acts as an uninsulated radiative heat shield within its allowable temperature range. Steady state creep data are widely published for different aluminum alloys. Cyclic creep information is not so frequent. Three (3) sources of high temperature creep data were found important for TPS design.

For the aluminum alloy 2024 (designation 24 S, [14]) cyclic prediction capability concerning varying temperatures and stresses, based on linear creep theory, has been identified for metallurgical conditions 0 (solution treated), T1 (cooled from elevation temperature and naturally aged) and T3 (solution treated and cold worked). Cyclic creep as a summation of steps of constant creep, reported as Robinson's method [14], can be adequately predicted up to the following maximum temperature levels: 300°F maximum for stress cycling at T1 and T3 conditions, up to 600°F for the 0 condition. Creep behavior under temperature cycling is equivalent to constant temperature creep at a maximum of 600°F and below in the T3 condition.

Four (4) static and cyclic tensile creep tests each per temperature-stress-endurance condition were conducted [12] for 2219-T78 aluminum with data reported highly scattered [Tab. 4]. 2219-T78 is a sheet or plate product, solution treated (tempered) at 995 °F, cold worked, and precipitation treated (aged): sheet at 325 °F for 24 hr and plate at 350 °F for 18 hr. Static exposure time was 180 min. Total cyclic exposure time was 270 min., 25 min. per cycle, with 150 min. at maximum conditions.

Aluminum alloy 7175-T736 is a premium die forging developed by Alcoa, a material in a favorably stable metallurgical state during high temperature use. Plastic deformation curves of .2% are presented [17] for up to 500°F and up to 1,000 hrs. No cyclic data are reported. At a steady stress level of 3.2 ksi at 500 °F, for instance, .2% creep occurs within 1,000 hr. Heat shield properties for this product were analyzed at a panel depth of 1.25 in. and a gage thickness of .0093 in. At 20% of deflection criterion "2", free-clamped support, a panel of 43 lb-in strength and 67000 lb-in<sup>2</sup> stiffness, weighing .4 lb/ft<sup>2</sup> carries a load of .6 psi at a panel length of 2 ft. Elastic deflection is .016 in. and plastic deflection is .08 in.

## 2. Beryllium in TPS Design

Beryllium (and René 41) radiative insulated shingles have been operational on the sides of the Mercury and Gemini re-entry vehicles [4]. Beryllium is advantageous because of its light weight of .066 lb/in<sup>3</sup> and as a good heat conductor leveling temperature gradients in the TPS. Oxidation protective coating requirements exist for a nominal penalty (~.005 lb/sqft).

The proposed manufacturing methods for rib stiffened design are welding or diffusion bonding [18]. Hat and vee corrugations could be spot welded to the face sheets. 5 x thickness of gage should be considered the minimum bend radius for vee corrugations. For smallest bend radii, forming has to occur around 1325°F. It is impractical for handling purposes to chem-mill .02" sheet thinner than .01" (10 mil). A very low R.T. Poisson's ratio of only .02 in short-transverse direction has been observed in .02 to .063 inch sheet due to rolling [19].

Hot cross-rolled sheet of up to 2% BeO content (melting point at 2340°F) has been considered for TPS design primarily due to its high stiffness at elevated temperatures. The disadvantage of 1000°F and up, however, is high creep. Steady-state creep resistance has been reported [20] for cross-rolled beryllium base 2% BeO sheet in transverse direction up to 800°F. Plastic .5% deformation (rupture) stresses at 800°F are 20 (27) ksi for 100 hrs and 15 (20) ksi

for 1000 hrs exposure, respectively. Other high temperature data available are short time secondary creep rates [21] for hot-pressed block beryllium, Brush Lot 4324. The lowest creep rate measured was .002 (%/sec) at 1.8 ksi and 1500°F, yielding .5% creep in .07 hrs. One-hundred hour rupture-life tests [22] as a function of temperature in a beryllium-beryllium carbide system of approximately one percent carbon content, indicate stress levels of .2 (.3) ksi at 1200 (1500) °F, respectively. These data sources [20, 21, 22] were extrapolated to project a 1.2 ksi stress level (or less) to cause .5% creep in 100 hrs at 1200°F. Weight estimation of a 1. psi-2 ft heat shield (100% FC-"2") reveals 2.78 lb/sq ft. Depth (gage) of the square channel cross section is .53 (.098) inch.

### 3. Titanium Alloys

Titanium alloys for load-carrying outer surfaces have been justified in SST concepts, experiencing 400 to 500°F in flight. They are useful for TPS at much higher temperature. Thin gauge single-face corrugation 20" by 20" panels, .01" skin to .005" corrugation, have been manufactured, using Ti-8Al-1Mo-1V [7]. Special machining, forming and joining technology has been developed to accomplish such task [23].

Quantitative variation of creep behavior ranks first when considered with variations of other mechanical properties important for design. Creep strength data for .01 to .5% creep of different titanium alloys at 500 to 1200°F and for up to 1000 hr. (and higher), from various sources, were found to vary drastically, with the alpha-type alloys generally having superior creep strength in the annealed condition. Strength is practically nil for Ti-6-4 beyond 900°F. Titanium alloys containing gallium are very promising [24]. Review of the results for twelve (12) alloys shows that the C1 alloy of composition, Ti-4.5Al-2Sn-3Zr-3Ga-1Mo-.5Si, exhibits superior tensile and creep resistance properties. Larson-Miller presentation for .2% plastic creep between 850 and 1100°F with stresses ranging from 25 to 85 ksi, shows the operating stress level of the C1 alloy approximately 10 ksi higher in comparison with the current most creep resistant commercial alloy 5621S. AF goals for high temperature creep strength were met with AF-1 (Ti-5Al-5Sn-2Zr-.8Mo-.5Si) [25], commercially not available. Representative data of .2% steady creep of prime candidates up to 1000°F are compared with the two conventional Ti-6Al-4V and Ti-8Al-2Cb-1Ta alloys [Tab. 5]. The selective use of different titanium alloys under similar environmental conditions is not the only approach to TPS optimization. There are others, such as manufacturing considerations.

Precision casting of large thin-walled shapes has been proven technically and economically feasible. Steady creep data for up to 1000 hrs at .1 and .2% creep have been generated for these types of castings and for comparison of

Ti-6-2-4-2, Beta III, and Ti-6-4 [26]. Here, Ti-6-2-4-2 previously developed as a so-called "super" alpha alloy for engine use in bar, forging, flat-rolled and extruded product form is superior over the others. As an example, the Larson-Miller presentation of the standard products for .1% plastic creep at 1000 hrs reveals 48 ksi at 800°F, 23 ksi at 900°F, and 10.5 ksi tensile strength at 1000°F. For castings the data are 60, 33, and 16 ksi, respectively, which is an improvement of 25%, 43% and 52% over the other manufacturing methods.

Second important were found variations of specific weights due to high percentages of alloying constituents, and elastic moduli in tension and compression. For example, Ti-8Al-2Cb-1Ta 5/8" annealed bar weighs .156 #/in<sup>3</sup>, and Ti-11Sn-5Zr-2.5Al-1Mo-.25 Si (Ti-679) .174 #/in<sup>3</sup>. For Ti-6-4 T-extrusions [27] at 800°F, the compression modulus is 24% higher than in tension. This percentage increases with the temperature going up.

Creep strength data for simultaneous cyclic temperature/load conditions are unfrequent. Robinson's method [14] to predict creep due to temperature cycling at a steady stress level, based on steady-state data was found feasible up to 800°F for the alloy, 130A.

The following "short time" creep results (equivalent to 13 re-entry cycles) indicate that cyclic creep is a design critical problem at 900°F and up [12]. Static and cyclic tensile creep tests were performed for Ti-6Al-4V (STA) at an exposure of 900°F, 23(ksi) for 225(min) total static time, and 195(min) at max. conditions with 25(min/cyc), 325(min) total cyclic time. Creep data reveal a wide scatter and cyclic degradation [Tab. 6] as compared with .002 (in/in) estimated from handbook data. No indications of degradation in fracture toughness,  $K_{IC}$ , at R.T. and residual strengths,  $F_{tu}$ , at R.T. and 600°F due to cycling were observed.

The weights for TPS panels made of a titanium alloy have been determined [Tab. 7] .72 to 1.05 #/ft<sup>2</sup> in the temperature range R.T. to 850°F for a .5 to 2. psi limit pressure differential and two different designs, MSFC and Phase B. These data lack complete description of input parameters for comparison with weights of the method established, and are at least 10 times higher than theoretical prediction for the 20 in. span panel below the minimum gage limit [Fig. 14 and 15] indicates.

#### 4. Superalloys and DSM

TPS designs of superalloys, René 41, TD-Ni Cr, H 188 and Hast X, for 100 re-entry cycles (ca 50 hrs) are limited by cyclic creep strains [8], that are anywhere from 3 to 10 times as high as predicted from steady-state creep tests [Tab. 8]. Degradation of R.T. tensile strengths is also more severe due to cyclic creep, a phenomenon not yet understood.

The dynamic oxidation behavior at 2200°F of several dispersion-strengthened nickel-base super alloys, iron-base and nickel-base super alloys has been investigated by NASA Lewis Center [4]. One hundred test cycles of 30 min., each at 2200°F and 10 torr air pressure, followed 6 min. cooling intervals. The 7-20 torr pressure range would be experienced by the shuttle. Total metal loss for most of the tested alloys was well within re-use limits. The investigation covered oxidation rate, vaporization rate, spalling rate and grain boundary attack.

### Nickel Base Alloys

High temperature nickel base alloys, wrought or cast, selectively contain Cr, Co, Mo, W, Nb, Ti, Al, Ta [28]. Cyclic creep, more representative for typical flight conditions than steady creep, of René 41 and Hastelloy X has been identified by test to occur several times higher than steady-state creep [Tab. 8]. Previous experience with Inconel X reveals [14] that prediction of cyclic creep from static data is adequate up to 1500°F for this alloy. Precision cast, structural concepts of In-100 have been experimentally verified [10] to possess unique high temperature creep capabilities superior to those of other fabrication methods. Comparing steady-state creep data, cast In-100 and cast Inco 713 LC are superior up to 1800°F, with Hastelloy X, Inco 718, Incoloy 901, Nimonic 80A and René 41 having inferior creep strengths in that order.

The GE "René" Alloy 41, also known as Haynes Alloy No. R-41, vacuum-melted and of Ni-19Cr-11Co-10Mo-3Ti-1.5Al composition, is in solution heat-treated and aged condition one of the strongest alloys available for non-cyclic use in the temperature range of 1600 to 1800°F. At these temperatures, it is reusable at much lower stress levels under shuttle conditions [8]. Experience exists for application on the sides of the Mercury and Gemini re-entry vehicles.

R-41 is available in all wrought forms, as precipitation hardened thin gage sheets and also as vacuum investment castings [9, 10]. Minimum gages were manufactured [7] for .002" corrugations in stiffened sandwich panels with .01" skins. T-sections of 18" span were fabricated initially of .025" sheet E. B. welded, creep flattened, and chem-milled to .01" with the weld and flat surface area mask off. Then panel fabrication by welding of ribs was developed for .005" minimum gages. A single-faced flat corrugation-stiffened 12" x 20" panel using .005 skin and corrugation was spot welded and heat treated. The warping stayed within allowable limits. Diffusion welding is typically possible at 2000°F and 10 ksi.

The effect of multiple re-entry on creep in tension for 100 cys. with duration of 1/2 hr each has been determined at a stress level of 8.5 ksi and 1600°F for two types of heat treatment [Tab. 8]. The 2050°F solution treatment, 1650°F aging, is superior to the other one (1400°F age) reported [Fig. 3]. The ratio of predicted-to-actual creep for this 100-cyc. interval remains fairly constant at 1 to 13.3. TPS design was found feasible at the reported 8.5 ksi stress level

at 1600°F and not identified below the 2.ksi at 1800°F, where the actual 100 cycle elongation hardly exceeds .5%, the characteristic limit found by the creep-index criteria established in section III. Loss of strength occurs through overaging at 1800°F rather than oxidation [8]. The oxidation resistant material experiences a slightly greater property degradation at one atmosphere than at high altitude pressure.

Due to lack of cyclic creep data at several stress levels, a stress level variation was performed at 100 hrs and 1400°F with steady-state data for René 41 revealing .02, .05, .1, .2, .5% strain at 9.2, 14., 22., 32., 56. ksi respectively. Design curves of type [Figs.6-8] applied at constant weight and panel depth show TPS optimization to extend from moderate panel lengths and high pressure levels to larger panel sizes at lower pressure loads. Thus, a decrease of excessive loading capacity can be traded against longer panels by using 10 to 20 times smaller creep rates with no weight penalty involved.

The typical dimensions of a hat section panel weighing 1.1 lb/ft<sup>2</sup> are: gage thickness .008", panel thickness .3", hat distance 1.2", hat size at the top 1.", and .44" at the bottom. TPS weights independently have been estimated [Tab. 7] for the temperature range 800 thru 1600°F, to reach 1.1 #/ft<sup>2</sup> for .5 ksi and 1.8 #/ft<sup>2</sup> for 2 psi, both at 1600°F. The same source quotes the MSFC TPS weight 1.95 #/ft<sup>2</sup> fairly high at 1300°F.

The 100 cycle unit area weight per psi pressure load and per ft panel span for the square channel cross section at a criterion of 2/100 of panel length total deflection, using the creep data [Tab. 8] at 1600°F (2050°F sol., 1650°F age), is estimated .54 #/ft<sup>2</sup>/psi-ft with gage thickness increasing at the rate of .0042 in/psi and panel depth at the rate of .43 inch/ft of panel length. Using as material data the empirical creep-temperature-stress functional relationship of [9], however at 100 hrs, same temperature, and a fixed 1. inch panel depth, gage thickness and weight are .0073 inch and .94 #/ft<sup>2</sup>, respectively, at a match of the remaining parameters of both the approaches with each other. The relationship gage-portion-to-weight, would bring the equivalent gage thickness of the 1.8 #/ft<sup>2</sup> panel [11] up to .014 inch, which thickness was not reported.

Hastelloy X (Ni-22Cr-18Fe-9Mo-1.5Co-.5W), available in wrought and cast conditions, has excellent forming and welding characteristics. Thin gage manufacturing is feasible as thin as .002 in. for sandwich corrugations, and .01 in. for skins. Superior oxidation-resistant properties up to 2200°F are reported [28]. high metal loss of 2.65 mil per side, however, for TPS under shuttle conditions [4].

In annealed condition [29], this alloy was chosen in the GDC-columbium elevon of the CVL-4 vehicle exposed to a 1720°F peak temperature [3]. Hastelloy X has inferior steady-state creep resistance at 1350°F [10] compared with

In-100 and Inco 713LC. Cyclic creep reported at 1800°F and 2. ksi for 100 cycles [Tab. 8] is too high for TPS design. Stress levels applied smaller than 2. ksi, data of which were unavailable, may turn out too heavy TPS at 1800°F.

Haynes In-100 is a vacuum-melted, vacuum-cast, nickel-base alloy of the aluminum-titanium, precipitation-hardening type and especially useful in high-stress applications at high temperatures. Possessing adequate oxidation resistance, the alloy can be used at temperatures near 1900 deg. F. Steady state creep data are reported for In-100 up to 1800°F, 1000 hrs. Present use is for turbine blades in the as-cast condition. Its composition: Ni-15Co-10Cr-5.5Al-4.7Ti-3Mo-.95V (Ref. Haynes), or according to another source (Ref. McDonnell) Ni-15Co-9.5Cr-5.5Al-5Ti-3Mo-.95V-.015B. Material density is .28 #/in<sup>3</sup>. An integrally stiffened panel with ribs in "quasi-isotropic" directions was vacuum cast [30] with as-cast web thicknesses of .03 in. and as-cast face sheet of .075 in. The outer surface was ground to provide a face thickness of 0.35 in.

The superalloy casting Inco 713 LC, Ni-13Cr-6Al-4Mo-2Cb-.7Ti is second after In-100 in creep performance at 1350°F [31].

The application of dispersion strengthened nickel-chromium has been estimated [32] to fill the gap above the 1850°F use temperature of superalloys and below the 2200°F lower use temperature of coated refractories. 85 to 95% of the orbiter external surface area will be below this max. use temperature.

Mechanical and physical property characterizations from R.T. to 2400°F for thoria-displaced nickel-chromium (TD Ni-Cr) sheet (Ni-20Cr-2ThO<sub>2</sub> and other compositions) of varying heats (micro-structural changes) and different gage thicknesses exist from different sources [8, 33, 34]. At elevated temperatures meaningful reproducible creep strengths are high, along with low ductility and anisotropic response. The creep mechanisms (2 or more) and micro-structural variables are unidentified. At operating temperature ranges and stress levels reported [Tab. 8], deviations between predicted and actual creep elongations are moderate, lowest as compared with all the superalloys investigated [8]. The same is valid for effect of cyclic exposure on residual strength reduction. TD Ni-Cr possesses excellent oxidation resistance.

TPS panels of annealed TD Ni-Cr sheet material have been manufactured with bent radii of 3x-the-gage thickness formed at R.T. Gage thicknesses reported [29] are minimum gages of .008" for skins and corrugations and .002" for sandwich corrugations. In one program [35], surface treatment was cleaning, grid blasting and preoxidizing at 2000°F. Diffusion welding is technically feasible with a typical bonding pressure of 5 ksi for 2 hrs at 1900°F. Joining with fasteners of TD Ni-Cr [4] is unreliable due to popping of heads along



the coldworked and recrystallized areas of the heads which results from the head upsetting operation.

Although not dealing with typical re-entry TPS panels, a test program has been completed and evaluated [35]. Structural panels of  $1.68 \text{ \#/ft}^2$  reacted loads of the primary structure, to which they were attached by flush head screws, and those of thermal expansion differences. The fin primary structure and surface stiffened skin for the FDL-5A vertically boosted earth-orbital vehicle, having nominal re-entry time of 60 to 90 min. has been designed and tested under max. temperature of  $2240^\circ\text{F}$  for thirty  $\frac{1}{2}$ -hour thermal cyclic conditions without failures. The single-faced, corrugation-stiffened TD Ni-Cr panels, with face sheets .015 in., corrugation .01 in. and edge members .02 in. thick, shallow beaded to prevent buckling, and with detail parts assembled by spot welding, were capable to sustain the repeated cycles of the normally and chordwise not equally distributed point loading introduced into the primary structure without buckling.

A TPS system consisting of a .2" flat fluted skin of recrystallized TD Ni-Cr backed by a Dyna Flex insulation [3] has been cyclically tested in a radiant heat lamp facility at atmospheric pressure. The panel was loaded by drawing a pressure differential of .1 psi at the panel back face. Test cycles totaled 50 of 2/3 hr trajectories at max. temperature of  $2200^\circ\text{F}$ , 10 hrs total exposure time above  $2000^\circ\text{F}$ . Small buckles occurred after 10 cycles due to configuration imposed thermal stresses, and cracks after 25 cycles. The test panel experienced a structural vibration and acoustic environment.

TPS analysis has been performed [7] for short and long cross range shuttle vehicles, using hat and rib stiffened TD Ni-Cr panels. For the short cross range vehicle, panel location at the bottom centerline, the hat corrugation was reported with dimensions: 1.2" hat size at top, .85" hat size at bottom, .29" panel thickness, and .008" gage thickness, constantly weighing  $1.2 \text{ \#/ft}^2$  between 1400 and  $2200^\circ\text{F}$ . The basic weight of a similar hat section for the long cross range vehicle has been determined  $1.3 \text{ \#/ft}^2$ , increasing to  $1.55 \text{ \#/ft}^2$  at  $2200^\circ\text{F}$ . Both types of panels were designed for a total of 100 flights with the panels at max. temperature for several minutes. Linear thermal expansions have been reported for the 30 in. long panel: .35, .55, and .8 in. at 1400, 1800, and  $2200^\circ\text{F}$ , respectively.

The TPS weights calculated for free-clamped support, 100% of deflection criterion "2", and the fixed stress levels and indicated temperature ranges [Tab. 3] 6.5 ksi at  $1800^\circ\text{F}$ , 5.ksi at  $2000^\circ\text{F}$  and 3.5 ksi at  $2200^\circ\text{F}$ , are 1.76, 4.06 and  $6.67 \text{ lb/sqft}$  per 1. psi pressure load and 1. ft panel length ( $\text{lb/sqft/psi-ft}$ ), respectively.

#### Iron-base Superalloys and Stainless Steels

Robinson's method for cyclic creep prediction using steady-state data was reported for some steels [Tab. 9]. The A-286 steel was used in the CVL-4 Convair Vehicle [3].

### Cobalt-base Alloys

Data on rupture strengths of cobalt-base alloys between 1200 and 2000°F for 100 and 1000 hrs are reported [36]. Highest creep resistance at 2000°F was experienced with the NASA Co-W-Re alloy for high temperature space applications: 6.3 ksi for 1000 hrs, 9.7 ksi for 100 hrs. These rupture strengths at 2000°F are low when compared with columbium alloys (D-31 elongates 5% in 1000 hrs at 20. ksi).

TPS design with L-605 and/or H-188 has been conducted by at least five different industries: General Dynamics Convair, McDonnell Douglas Eastern Div., McDonnell St. Louis, Grumman Aircraft Co., and Boeing.

The commercially available cobalt base alloy, L-605 with other designations, Haynes 25 or Crucible Alloy WF-11, of composition Co-20Cr-15W-10Ni, is resistant to oxidation and carburization at 1900°F. Normal use in jet engines and furnaces is in the temperature range 1400 to 1600°F, and 1600 to 1900°F in emergency. This material possesses excellent workability, machinability and weldability. Tab. 10 reflects minimum gages.

For an eleven design peaking at 1900°F, L-605 was chosen by GDC [3]. At this temperature, the sheet has a 100 hr stress-rupture strength of 7,000 psi. Steady creep data of .5% were used for design analysis, as available for annealed sheet of .02 to .08 in. [5,9].

Haynes 188 is the L-605 alloy with addition of lanthanum for oxide stabilization. The melting point is at 2400°F. Heat oxidized for 1 hour at 1600°F, 22 ksi UTS at 1800°F was measured by McDonnell Douglas East. UTS is 30 ksi according to the manufacturer. Yield strengths at 1800°F are 20 (McDonnell) and 18 ksi respectively.

A beaded skin and hat corrugated heat shield of L-605 Tab. [11] has been designed and manufactured for temperature up to 1800°F weighing 1.25 #/ft<sup>2</sup>. Design principles have mostly been necessitated by experimental test, i.e. expansion joints were needed at the two ends, because of thermal growth in longitudinal direction only. The lateral thermal expansion is absorbed by rising of the beads. Therefore, size limitation in lateral direction is restricted to sheet sizes available. Thermal expansions measured are similar to those of TD Ni-Cr. A span of 20 in. was found acceptable to provide local and overall stiffness, to prevent flutter, to have panels easily removable for maintenance and inspection, and to cause minimum leakage at edge seals.

The Haynes-25 panels [11], No. 2 of 18 in.x18 in. size [Tab. 11] and No. 3A of 20 in. span, for the low L/D and high L/D orbiter vehicles, respectively, were supposed to yield center creep deflections ( $\leq$  aero limit) of .325 in. and .2 in., respectively, after 100 missions of 15 min. each. Uniform load of 40 psf was applied during each cycle at 1800°F. Panels were designed, using steady creep handbook data, such that a 3.75 ksi stress level generated a total of .4% creep in the extreme fibers. Panel No. 2 had .266 in. center deflection after 9 cycles and No. 3A had 1.25 in. after 22 cycles. Constants in two different cyclic creep laws (Nadai and Pao-Marín) were determined from

.008" sheet specimens cycled at stress levels between 1. and 8. ksi at 1800°F. The creep laws used in the contractor's creep deflection analysis of residual stress capability matched the results of the two heat shield experiments. Further study revealed that for a high L/D vehicle the allowable extreme fiber stress for meeting the required .25 in. permanent deformation per 20 inches is only 1.85 ksi. The stress level is 2.7 ksi yielding .1% creep in the case of the low L/D panel.

Required panel weights relative to pressure loads and specific design conditions for temperatures up to 1800°F are provided by another data source [Tab. 7]. Although data on hand are inadequate to conduct a perfect comparison with the prediction method developed, this was partially undertaken applying the cyclic creep data for H-188 [8] to generate unit weight vs. pressure load. The predicted unit weights for .5 and 2. psi [5] are much lower than the 100 cycles-exposure curve indicates.

## 5. Refractory Alloys in TPS Design

Refractory alloys provide the best creep resistances achievable at extreme temperature endurences. Operational experience with thin wall sheet and tube applications in reactors exists. Multi-source joining, welding, brazing and diffusion bonding parameters are available [4].

For a "theoretical" design trade-off comparing for instance the creep performance of coated tantalum alloy T-222 at a constant stress level of 12. ksi, and 2400°F for 100 hrs with coated columbium alloy Cb-752 [9], T-222 has 6 x higher creep resistance (1.%), 4.45 x higher stiffness ( $22.2 \times 10^6$  psi), however, is about 1.85 x heavier (.604 #/in<sup>3</sup>) than Cb-752. The molybdenum alloy, TZM (.369 #/in<sup>3</sup>), slightly heavier than columbium, shows excellent creep rupture performance [9], 42 ksi for 10000 hr at 2000°F. For some refractory metals and alloys [37], biaxial stresses and creep strains were compared with uniaxial creep data of other investigators for ranges of temperature 1950-3000°F, stresses .4-32 ksi, creep rates  $10^{-3}$  to  $10^{-6}$  in/in-hr and test duration 100-1000hr. The biaxial and uniaxial creep properties were found equivalent on the basis of effective stress and strain rate as defined by the von Mises criterion for plastic flow.

Usage in TPS is limited by oxidation (burn-up) as well as exceeding of deflection limits, whatever happens first. Coating systems against oxidation, functioning a few minutes up to above 100 hrs, have been developed for columbium and tantalum alloys, being less advanced for the latter ones. Problems are with coated and threaded refractory fasteners for shuttle requirements [4]. Coatings on the threads fail under very low torque levels and where heads are gripped by driving devices. In addition, control of thread tolerances due to coating thickness is marginal.

## Columbium Alloys

The approximate maximum use temperature for coated columbium alloys has been reported at 2370°F with 90 to 98% of a typical orbiter external surface

area below this temperature [32]. Typical TPS alloys with coating potential are Cb-752 (.343 #/in<sup>3</sup> uncoated, .325 #/in<sup>3</sup> coated with VH-10 [29]), C-129Y and FS-85 [10,38]. C-129Y possesses mechanical properties similar to those of Cb-752, however, better forming characteristics [3]. Coated Cb-103 evaluated for space shuttle use by Boeing (IRAD) revealed high inspection costs.

One of the earliest columbium creep bending tests conducted [15] was the 4-point loading of a 11.5 in span cross sectional U-channel. After 32 minutes, maximum allowable plastic deflection was reached at a max. bending moment of 110.2 #-in. Other short time studies at high temperature with rib-stiffened and corrugation stiffened TPS panels made of .012 in. columbium alloy sheet revealed weight vs. allowable moment data [7]. A pi-strap staggered TPS concept was developed for use at the bottom location of a long cross range vehicle for peak pressure loads of .4 and 2. psi and up to 2200°F. The vee-corrugation stiffened panel in flight direction was clamped between the external pi-straps and panel stiffener in cross flow direction. Design features included connections to adjacent panels, mid panel supports and thermal growth accommodations. The panel of coated FS-85, .68 inch thick, of a .008 inch gage material, vee-distance at 1.2 inch, and designed for an ult. bending strength of 147 #-in at R.T., weighed 1.84 #/ft<sup>2</sup>. Residual tensile yield strength at R.T., under the scope of this program, was determined on Cb-752, coated with R 512 E Sylvania, and found to decrease approx. 20% from its original strength after up to 100 creep cycles under shuttle conditions. The other design concept of rib-stiffened coated columbium was a flat surface panel stiffened by weld-on ribs of equal depth and spacing, oriented in flight direction. Bolts and integral spacers connect this panel through the skin with an angle member mounted on a rib stiffened hat type edge support clip, providing connections to the adjacent panels of similar construction, and elliptical hole type thermal growth accommodations. Another hat sectional support clip furnishes a lateral attachment mid point to a channel panel center support member. On the forward and one lateral side of the panel, a shingle type overlap exists to the adjacent panels. All clips functioning as attachment points are part of the load carrying substructural frame.

Much experience has been gained from the General Dynamics Convair hot structural elevon development for the CVL-4 vehicle [3]. This vehicle was originally designed for a factor of fatigue safety of 4 and/or allowable creep strain of 1.%. The elevon mostly consisted of Cb-752 and part of it of L-605 for the 1900°F and Hastelloy X for the 1800°F regions. The design was to sustain 2500°F short time peak temperature. The Cb-752 gage thickness utilized was .012 inch. Part of which was diffusion bonded with vanadium foil interleaf. Sinusoidal webs were welded as spars and ribs to leading edge and skins.

The CVL-4 elevon was tested [3] at angles, 0/5/10/15°, in the Convair SEAR hot gas (GO<sub>2</sub>/GH<sub>2</sub>) facility. Heat fluxes were up to 39 BTU/ft<sup>2</sup>-sec. Rivets used in the Cb-752 sheets experienced early service failures due to malfunctioning of their coatings. The rivets were said being damaged during the riveting process and not sufficiently repaired, such that coating spallation and oxide penetration due to turbulent conditions could occur. Coating investigations on C-129Y and Cb-752 material were conducted [3]. Fused slurry silicide coatings VH 101 (Si-Hf-Cr-Fe) and VH 109 Duplex (Si-Hf-Ta-Cr-Fe) of the Vac-Hyd Processing Corp. of Torrance, Cal. used for C-129Y oxidation resistance tests performed properly.

Testing at Convair was according to design specifications for the CVL-4 vehicle, 60 cycles of a 2400 sec trajectory, 2469°F peak temperature, 48.6 hrs of thermal exposure, 26.6 hrs above 2000°F. The TRW-pack cementation coating, (Cr-Ti)-Si, of the Cb-752 material failed on the CVL-4 structural component supplied to AFFDL for testing after 15 cycles of a 2400 sec trajectory, 5.3 hrs at 2000°F.

More confidence and competence in coated columbium has been established over the years. Fused slurry Si Cr Fe (R512E) coated Cb 752 showed satisfactory results in 50 or more high temperature lifting re-entry simulations at McDonnell Douglas [39]. Reuse is said to be limited now by creep deflection, not by any coating failure, even after deliberately inflicted damage to the coatings (up to 3/8 inch diameter). Ten (10) flights at least for coating re-usability at 2600°F were conducted. Plasma arc tests on coated columbium alloys under simulated space shuttle conditions by Battelle/Columbus [4] indicated that R 512 E and VH 109 coatings are protective up to 2470°F. They perform satisfactory for several cycles to 2400°F, but do not meet 100 cycle dynamic life. Coating failures marked visible by oxidation products and non-catastrophic for additional re-entries mostly occur at edges. More a problem exists with plasma ingestion after burning of a small hole, during an entry cycle, than by loss of strength or embrittlement.

The use of coated columbium panels would be risky as indicated without a repair technique developed by Sylvania [4]. This is considered a technical break-through because manufacturing and handling damage is a certainty. Inspection by autoradiographs and field repairs in less than 5 min. with a portable quartz lamp heater were found satisfactory for more than 100 cycles to 2400°F.

Diffusion bonding for shuttle hardware of columbium performed at the NAR Space Div. [4] appears sufficiently developed and offers several advantages over welding and brazing. The choice of the joining process, however, will depend largely on the design details. This company reported exceedingly low stresses at high temperatures for the design of a 18 in. x 36 in. test panel made from a .02 in. thick face sheet, chosen as the minimum gage allowable for production handling, stabilized by diffusion-bonded stringers. Maximum panel deflections resulted from thermal gradients in the first 300 sec of re-entry. Thus the panel was adequately strong to resist the maximum air load of 3 psi during boost at 70 °F.

The basic metallic unit weight of a columbium heat shield concept including clips and attachments was estimated 1.3 #/ft<sup>2</sup> [16], based on a comparative study on performance of active and passive TPS of the Lockheed delta-body orbiter for 1500 NM cross range. The windward surface area of 4455 ft<sup>2</sup>, 36% of total surface area, was considered under a re-entry plan-form wing loading of .34 psi at a smooth panel peak temperature up to 2300°F and local temperature as high as 2400°F. For increased stiffness, the outer panel was formed with circular arc corrugations using a pitch of 1.4 in and a height of 14 in. No further information on other TPS design parameters, dealt with in this study, was provided.

Other independent weight estimations of coated columbium TPS [5] indicate the weight between 1600 and 2400°F at the loading level of .5 psi to moderately increase from 2.2 to 2.4 #/ft<sup>2</sup>. The weight goes up from 2.3 to 4.05 #/ft<sup>2</sup> at the higher load of 2. psi within the same temperature range.

## Tantalum Alloys

The maximum use temperature for coated tantalum on the shuttle orbiter has been estimated at 2730°F [32], with approximately 95-98% orbiter area below this temperature. Problems are with the high creep rates and short coating lives at the temperature durables desirable.

To improve high temperature creep properties and still maintain good fabrication and weldability characteristics, the precipitation strengthened tantalum alloy, ASTAR 811C (Ta-8W-1Re-.7Hf-.025C), has been developed for nuclear power systems purposes [40]. Stress levels at temperatures for 1% elongation and 1000 hrs, as compared with T-111, are: 12 ksi at 2200°F and 11 ksi at 2400°F for ASTAR 811C (1 hour annealed), 18 ksi at 2200°F and 4.6 ksi at 2400°F for T-111.

Most of the extensive screening programs of tantalum coatings were conducted on Ta-10W test specimens. Coating performances [Tab. 12] are 50 hrs and up for a 2600°F, 10 torr cyclic environment [32], meeting the 100 cycles for the NASA shuttle [4]. The fused slurry silicide coating, 512C, appears to have re-use capability for only eight (8) to ten (10) missions at 2600 °F. An AF contractual requirement of 1969 [41] called for 1 hr at 3500 °F, having been surpassed by a TRW coating [42]. Data [42] are for unloaded specimens with 3 mils of coating, cyclic static oxidation tested in air. In case of the TRW W/Si<sub>2</sub> coating a max. high temperature life of 16 hrs at an optimum temperature of 3000°F was observed.

Heat shield weights of coated T-222 TPS concepts have been reported at temperatures up to 3500°F for short time loads, 1. to 4. psi, and under consideration of the total creep deflection allowable, .1 inch+.01L, as function of span, 1, 8. to 24. inch [15, Section IX-3, Structural Efficiency Studies]. The extreme operational environment was assumed totaling 50 hrs at 2500°F, 10 hrs at 3100°F and 1 hr at 3500°F for an average pressure load of 1.33 psi. The weight penalties estimated for 2. psi due to the allowable deflection limit [Tab. 13] reveal exorbitant increases when panel spans increase beyond 12 inches. The weights include supports and coating. Short time load deflection data up to 3500°F [15], not correlating with the assumed endurance environment, show as an example for an 8. inch long and 6. inch wide rib stiffened panel, weighing 4.5 #/ft<sup>2</sup>, under max. test load of 390# (ca. 8 psi), a permanent set of .625 inch, about 3.5 x higher than the allowable deflection.

Within the ranges of panel lengths and pressure loads reported, panel weights have been calculated, using T-222 creep data [15] of 10 hrs endurance at 2900°F, a stress level of 4.1 ksi yielding creep of .1%. Weights for a 2 inch deep hat corrugation panel were found to be a multiple of those reported [15].

Effective use of tantalum alloys as radiative heat shields is limited to hot spots on the vehicle, such as leading edges. Application oriented short span supports and additional cooling should be considered in terms of weight penalty trade-off and replacement intervals, respectively.

## V Conclusions/Recommendations

"Light weight" TPS design necessitates the consideration of plastic strain at elevated temperature. Estimated TPS weights found in references and methods of calculation used vary widely. Unit weights differ up to 100%, the cause of this variation could not be completely identified due to details missing in the multi-parametrical studies involved.

Material stress levels to design with are allowed to generate less than one half percent elongation due to plastic deformation over accumulated times up to 50 hrs or more. A background of experience exists with steady-state creep. Lesser attention is given to cyclic creep. Weight estimation with steady-state creep data is usually too low. Original cyclic re-use data only should be used for design purposes incorporating synergistic effects of temperature-load cycling.

The criterion of design applicable is the allowable aero-limit deflection at panel mid span as a direct result of cyclic creep elongation of the material. An analysis method for creep deformation was assessed based on simplified assumptions, moderate computational effort, and leading to a conservative estimate. Sixteen (16) important application-, configuration- and material-oriented design parameters were identified for effective radiative TPS design and used in the analysis. Four (4) methods of parametric modification for panel design optimization were found practical: stress-level, gage thickness, panel depth and allowable deflection trade-off. The potential of different existing high temperature metals was assessed with comparison of material systems valid only for identical temperature-endurances.

Design with aluminum alloys for temperature endurance is feasible up to 200°F. No long-time cyclic data for higher temperatures were found applicable. Use of beryllium is of disadvantage at 1000°F and up because of the high creep. Cyclic data for beryllium do not exist. For use of Ti-6-4, the strength beyond 900°F is practically nil. Titanium alloys containing alloying components such as gallium are effective for up to 1100°F. Cost consideration, however, should be a factor for specially alloyed titaniums. Cyclic creep of titanium is a design critical problem from 900°F up, which type of data is missing. Beryllium heat shields at moderate temperatures above 200°F are much lighter than those of titanium due to the higher strength/weight ratio of the beryllium. Based on the steady-state creep data available, beryllium panels have to be twice as heavy for the same performance because of the better creep properties of titanium at higher temperatures. TPS design with superalloys is limited by cyclic creep strains, 3 to 10 x higher as predicted from steady-state creep tests. Dynamic oxidation effects of superalloys stay within re-use limits. Precision cast nickel base alloys possess unique temperature creep capabilities superior to those of other fabrication methods. Under cyclic conditions, René 41 can be used at an unidentified stress level of below 2 ksi for 100 cycles at 1800°F. Application of the superior creep resistance of thin gage precision cast nickel base alloys should be justified from cost-effective manufacturing considerations. Cobalt-base alloys seem to be a replacement for nickel base alloys creep performance wise. Thorough testing and extensive analysis of TPS from Haynes 25 at 1800°F



revealed no extraordinary results. Dispersion strengthened nickel-chromium TPS fill the temperature gap above the superalloys and below the coated refractories. Typical basic weight for TD Ni-Cr TPS is reported  $1.55\text{#/ft}^2$  for 100 flights at  $2200^\circ\text{F}$  maximum temperature for several minutes. Cyclic stress level of 3.5 ksi at this temperature for material tested reveals creep too high for TPS design. Use of refractory alloys for TPS is limited by oxidation, as well as exceedance of deflection limits. Coatings developed are less satisfactory for the tantalum than for the columbium alloys. Maximum use temperature for columbium alloys is reported  $2370^\circ\text{F}$  experienced at the hot spots of a re-entry vehicle. Unit weights of columbium panels for use up to  $2400^\circ\text{F}$  rapidly increase with increase of pressure loading from 2 psi up. The best protective columbium coatings perform satisfactory for several cycles to  $2400^\circ\text{F}$ , but do not meet 100-cyc. dynamic life. The coating repair techniques developed can be considered a technical break-through. Problems of tantalum alloys are with high creep rates and short coating lives at the temperature endurance desirable. Coatings on tantalum alloys perform 50 hrs and up at  $2600^\circ\text{F}$ , 1 hr at  $3500^\circ\text{F}$ . Maximum use temperature for coated tantalum alloys is estimated at  $2730^\circ\text{F}$ .

Weight savings for hot radiative metallic heat shields primarily depend on minimum gage fabrication capability. Cyclic creep data accounting for synergistic effects of both temperature and load cycling are lacking for these thin gages. Other important data partly missing are oxidation effects and field repair. Use of TPS as an exterior component of moderate precision, attached to the surface of the vehicle, can be operationally very cost effective. The only source of TPS cost data available (Douglas data M 60892) is relative to 2024-T3 panels. Cost factor is 3 for René 41, and 4.5 for Ni-20Cr-2ThO<sub>2</sub>, up to 19 for the brazed concept, which means the choice of the manufacturing process is a determining cost factor.

Work beyond the scope of the current study. The required information for setting up effective test series of types of heat shields to be procured may be determined thru use of the analysis technique, i.e. influence of panel length on weight, selection of gages, and geometrical proportions for type of material to be desirable in a defined temperature range. Part of the panels should be tested to re-evaluate the basic material properties which could be different from available data used in the prediction method. Part of the testing should be performed in a high temperature static test facility and part of it in an arc heated tunnel [43]. As the duration of peak temperature in a tunnel run profile is usually shorter than the actual exposure during one flight cycle, more than one tunnel run has to be conducted on the test model.



### References

1. D.F. Adams, "Airframe Structural Materials for Drone Applications", R-581/4-ARPA, July 1971.
2. "Heat Shields", Unclassified NASA Abstract Bibliography, Oct 69 (over 700 unassorted refs.)
3. W.E. Black, "Space-Shuttle Vehicle High Temperature Load-Carrying Structure and Radiative Thermal Protection Systems", GDC-ERR-1497, Chapt. 4-Structures and Materials, pg. 3-14, June 1970.
4. L.J. Korb, "Heat Shield Materials Key to Space Shuttle", Metal Progress, Apr 1972.
5. E.E. Engler, C.E. Cataldo, "Design and Test of Advanced Structural Components and Assemblies", NASA TM X-2273, March 1971.
6. G.L. Palcheff, G.R. Gaumer, "Structural Thermal Protection Systems Criteria", McDonnell Aeronautics Co. Memo No. MRS-71, 1967.
7. J.K. Lehman, "Trade Studies of Thermal Protection Systems (TPS) Applicable to Shuttle", McDonnell Douglas Astronautics Company, Eastern Div., Nov 1969.
8. J.W. Davis, "TPS Metallic Materials Data", McDonnell Douglas Corp.
9. MIL-HDBK 5, Department of Defense, Washington D.C. 20025, 1972.
10. Aerospace Structural Metals Hdbk, AFML-TR-68-115, 1972 Publ.
11. H.G. Harris, K.N. Norman, "Creep of Metallic Thermal Protection Systems", NASA Space Shuttle Technology Conference at Langley VA, Vol II-Structures and Materials, NASA TM X-2273, March 1971.
12. G. Ecord, "Static and Cyclic Creep Exposure Test Results for 6Al-4V (STA) Titanium Alloy", NASA-MSc, Dec. 1971.
13. A.I. Smith, A.M. Nicolson, "Advances in Creep Design", Chapt. 21, Halsted Press Div., John Wiley, NY, 1971.
14. I. Finnie, W. Heller, "Creep of Engineering Materials", McGraw-Hill Co. Inc., NY, 1959.
15. R.E. Jackson, A. Lopatin, "Tantalum Systems Evaluation", AFFDL-TR-70-33, Apr 1970.

16. H.D. Schultz, F.L. Guard, "Comparison of Active and Passive Thermal Protection System Weights for a Delta-Body Orbiter", NASA Space Shuttle Technology Conference at Langley VA, Vol II-Structures and Materials, NASA TM X-2273, Mar 1971.
17. Battelle/AFML Data, Contract F33615-69-C-1115.
18. J.M. Finn et al., "Design, Fabrication and Ground Testing of the F-4 Beryllium Rudder", McDonnell/AFFDL-TR-67-38.
19. Materials Properties Handbook, Vol IV, Chapt. 13, North American Aviation, Los Angeles Div.
20. DMIC Data Sheet, "Base Material Beryllium Metal or Alloy 98Be-2BeO", AF 33(615)-2494, Jul 1966.
21. M.J. Rebholz, "Effects of Metallurgical Variables on Elevated Temperature Creep of Hot-Pressed Block Beryllium", LMSC-6-78-68-39.
22. J. Greenspan, "Stress-Rupture Properties of Beryllium Containing Carbide and Oxide Dispersions", Nuclear Metals, Inc., Concord, Mass., Rpt. NMI-1227, Mar 1960.
23. Defense Metals Information Center, "Aircraft Designer's Handbook for Titanium Alloys", AFML-TR-67-142, Mar 1967.
24. C.E. Shamblen, T.K. Redden, "Creep Resistance and High Temperature Metallurgical Stability of Titanium Alloys Containing Gallium", Metallurgical Transactions, Vol. 3, May 1972.
25. H.B. Bomberger, "High Temperature Titanium Alloys", RMI Co. Data, NASA-LRC Info. Exchange, Dec. 1971.
26. Rpt. IR-162-0(1), AFML Manufacturing Techn. Div., June 1970.
27. Battelle Columbus/Ohio, "Ti-6-4 T-Extrusion Data Sheet".
28. DMIC, "Description and Engineering Characteristics of Eleven New High Temperature Alloys", Memo 255, June 1971.
29. General Dynamics/Convair Rpt. ERR-1272.
30. R. Johnson, Jr., D.H. Killpatrick, "Cast In-100 Integrally Stiffened TPS Panel", McDonnell Douglas Western Div., AFFDL Presentation, Feb 71.
31. Abex, Mahwah, N.J., "Manufacturing Process Development for Super-alloy Cast Parts", Rpt. IR-8-297, AFML-MAT.

32. R.W. Hall, "Metallic Heat Shields Materials for Space Shuttle", NASA Space Shuttle Technology Conference at Langley VA, Vol. II-Structures and Materials, NASA TM X-2273, Mar 1971.
33. J.D. Whittenberger, "Creep of TD Ni-Cr", NASA-Lewis Research Center, Dec. 1971.
34. R. Johnson, Jr., D.H. Killpatrick, "Dispersion-Strengthened Metal Structural Development", AFFDL-TR-68-130, Part I, Jul 1968.
35. R. Johnson, Jr., C.L. Ramsey, "Design Manufacture and Testing of a TD Nickel-Chromium Structural Assembly", NASA Space Shuttle Technology Conference at Langley VA, Vol. II-Structures and Materials, NASA TM X-2273, Mar 1971.
36. W.F. Simmons (Battelle Columbus/Ohio), Metal Progress, Mar 1971.
37. W.L. Maag, W.F. Mattson, "Experimental Biaxial Creep Data for Tantalum, Molybdenum and T-111, TZM, TZC", NASA TM D-6149, Feb 1971.
38. General Dynamics, "TPS Metallic Radiative Thermal Protection System", NASA Contract NAS 1-9793, 1971.
39. AFML Material Briefs No. 5, May 1971.
40. R.W. Buckman, Jr., R.C. Goodspeed, "Precipitation Strengthened Tantalum Base Alloy, ASTAR-811C", Westinghouse Astronuclear Lab., NASA CR-1641.
41. D. Boyd, "Tantalum System Evaluation", Final Oral Briefing at Wright Field, Jul 1969.
42. J.C. Ingram Jr., R.J. Gran, "Assessment of Technology Status on Protective Coatings for Tantalum Structures", AFFDL-TR-69-12, Nov 69.
43. "AF Technical Capability Key", AFSCP 80-3, Sep 1967.

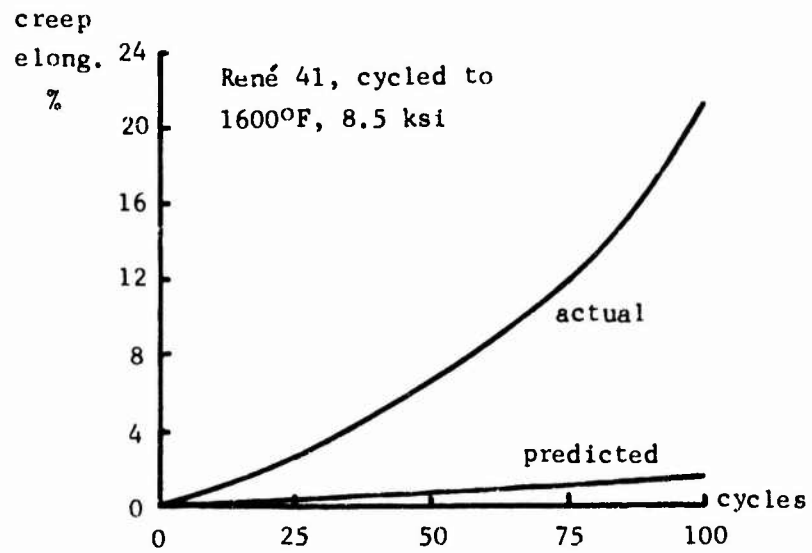


Fig. 1 Effect of multiple re-entry on creep [8].

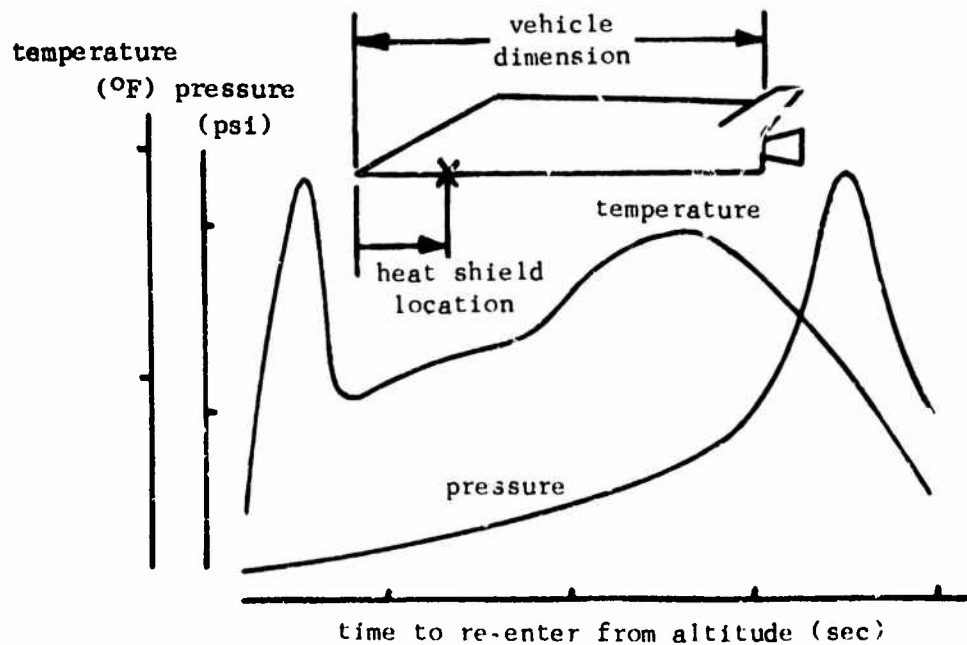


Fig. 2 Load-temperature profile.

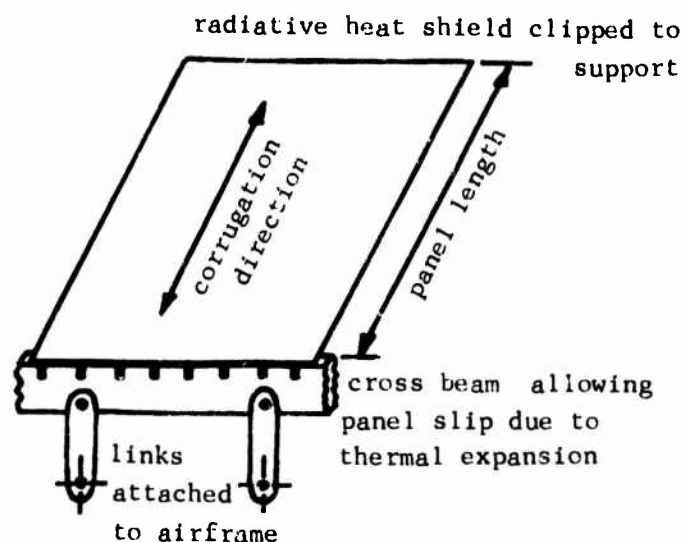


Fig. 3 Typical heat shield with support structure.

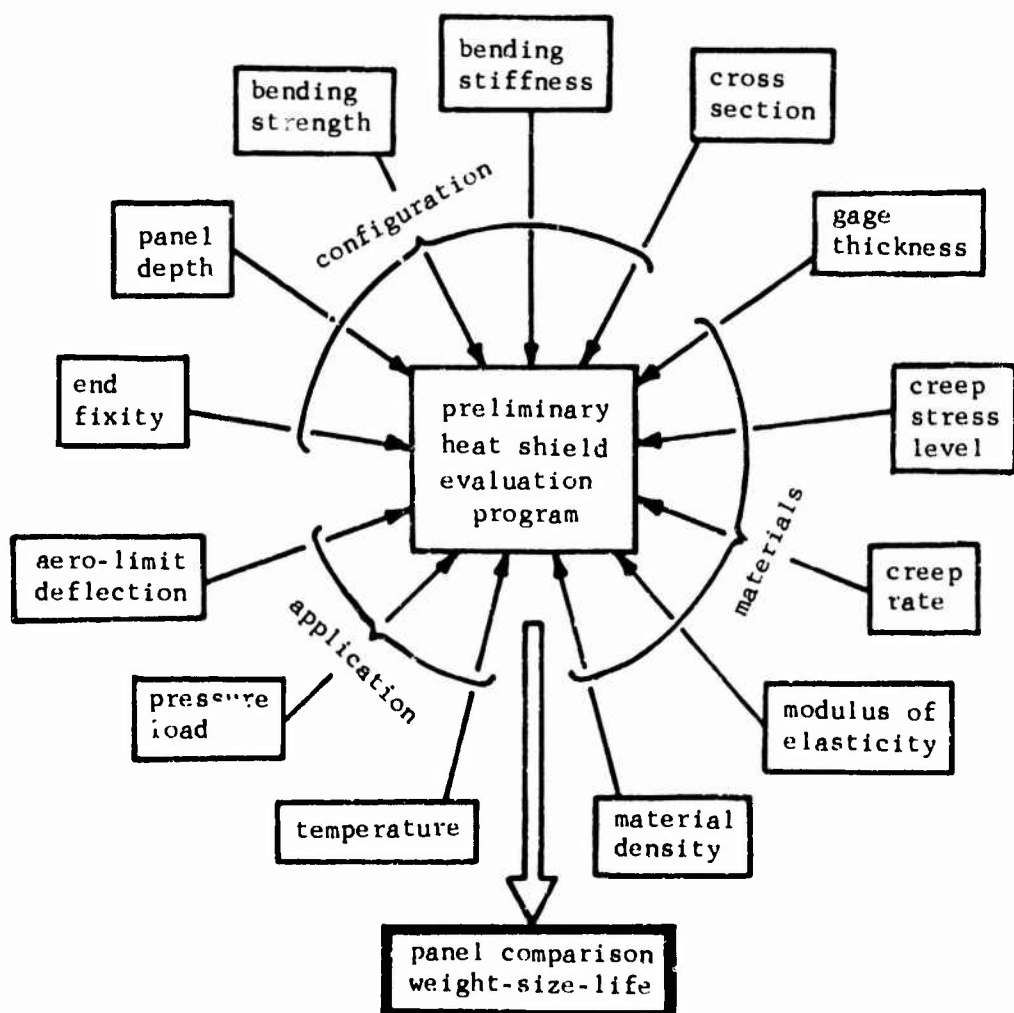
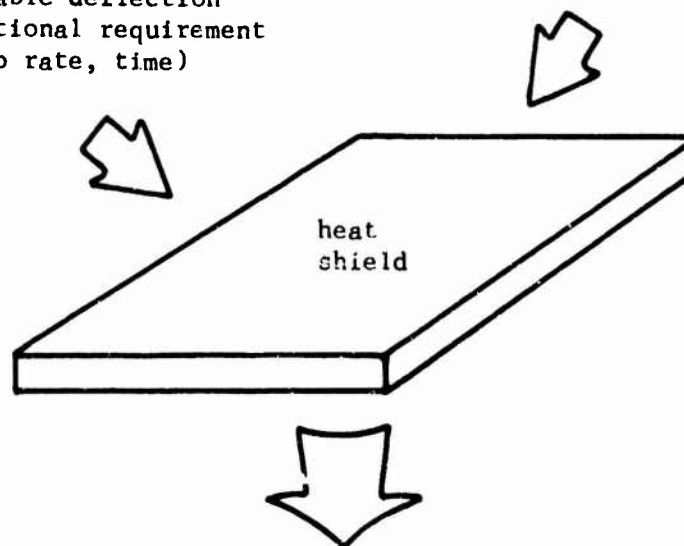


Fig. 4 Parameters for heat shield design.

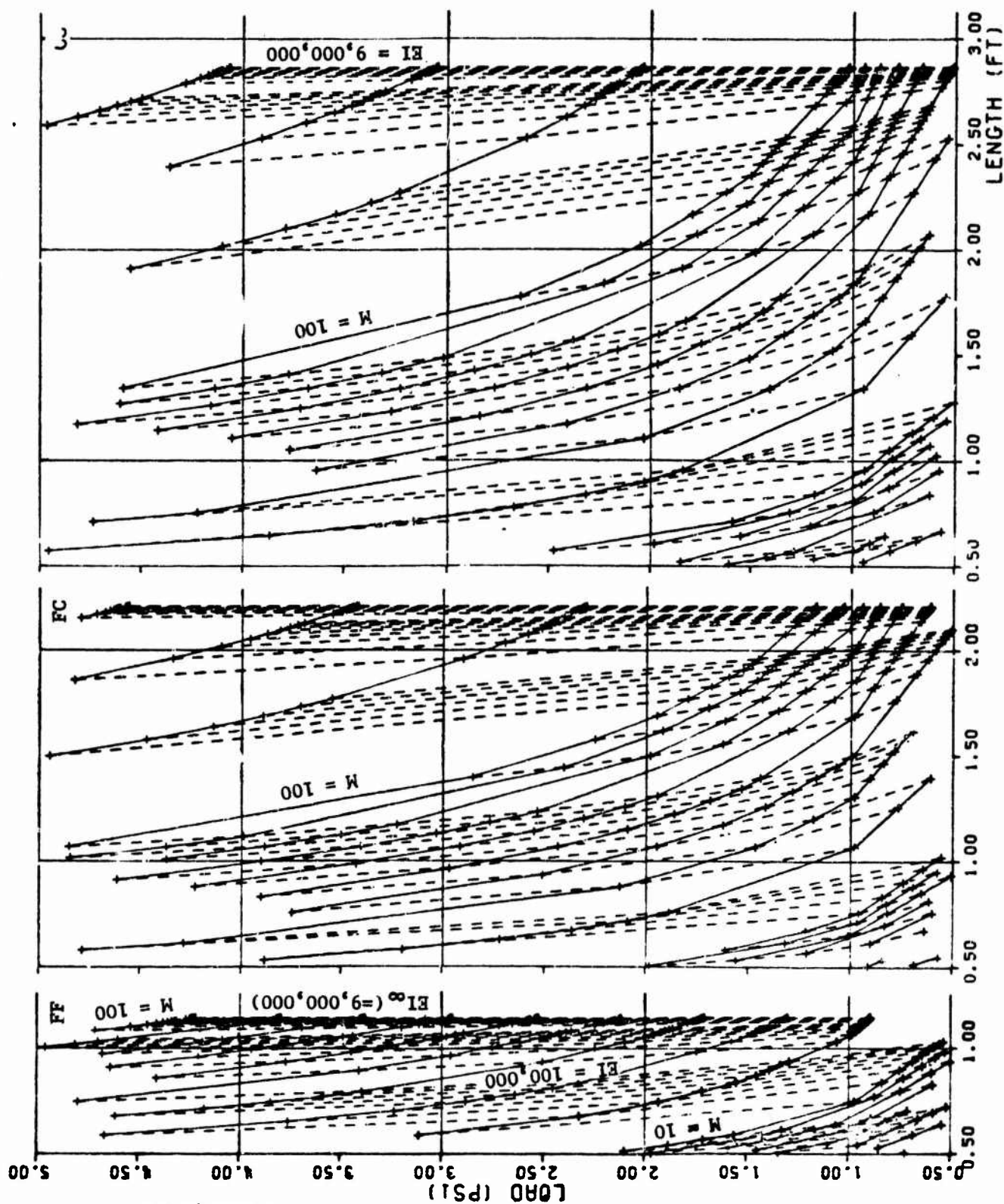
vehicle defined  
allowable deflection  
operational requirement  
(creep rate, time)

engineer selected  
bending strength  
stiffness (EI)  
end fixity  
panel depth



sizing parameters  
panel length  
pressure load

Fig. 5 Application fixed algorithm "1".



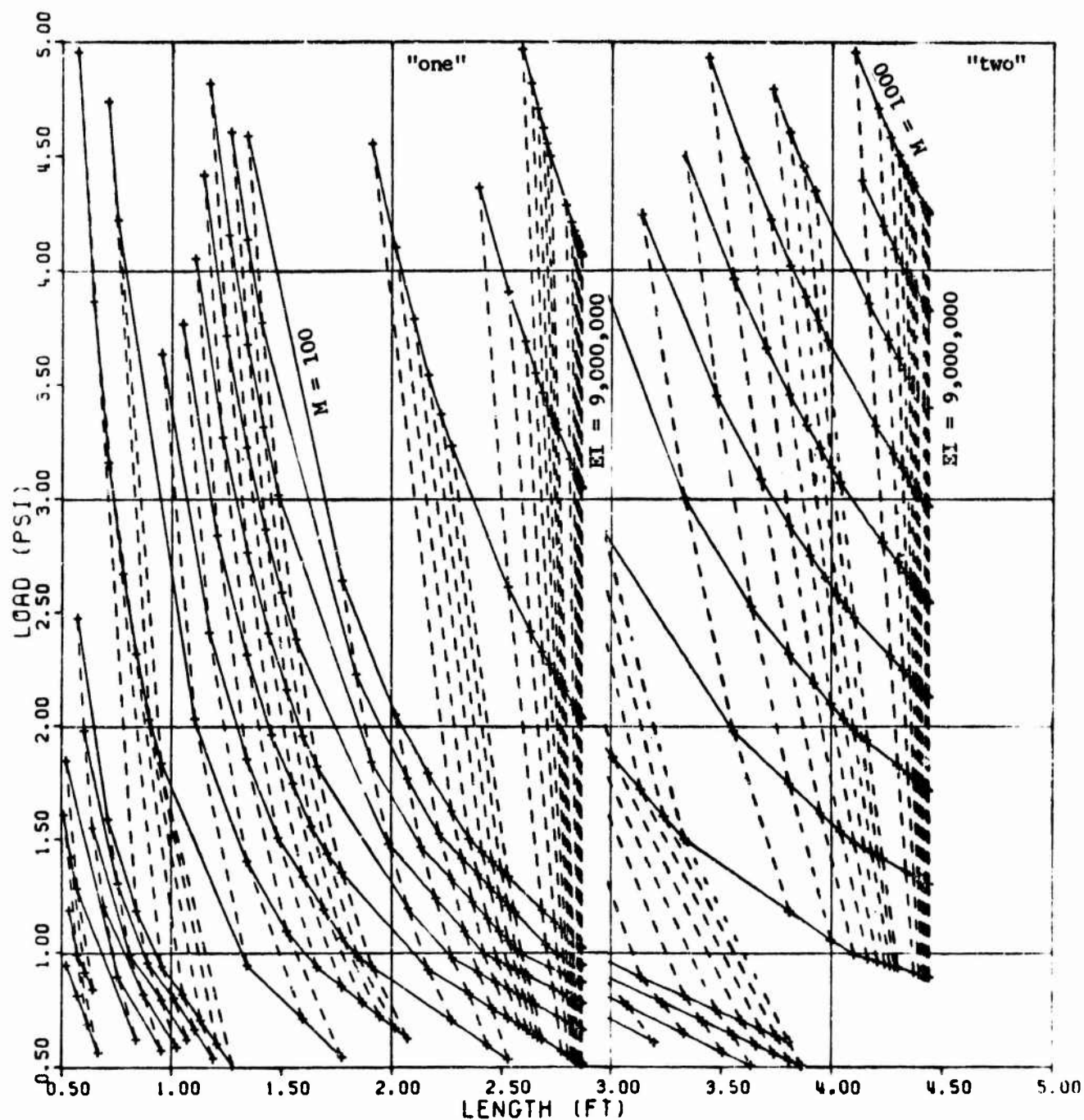
attachments:

free-free support, free-clamped support, clamped-clamped sup.

creep condition:  $.003 \text{ in}^{-1}$

deflection criterion: 50% of "one"

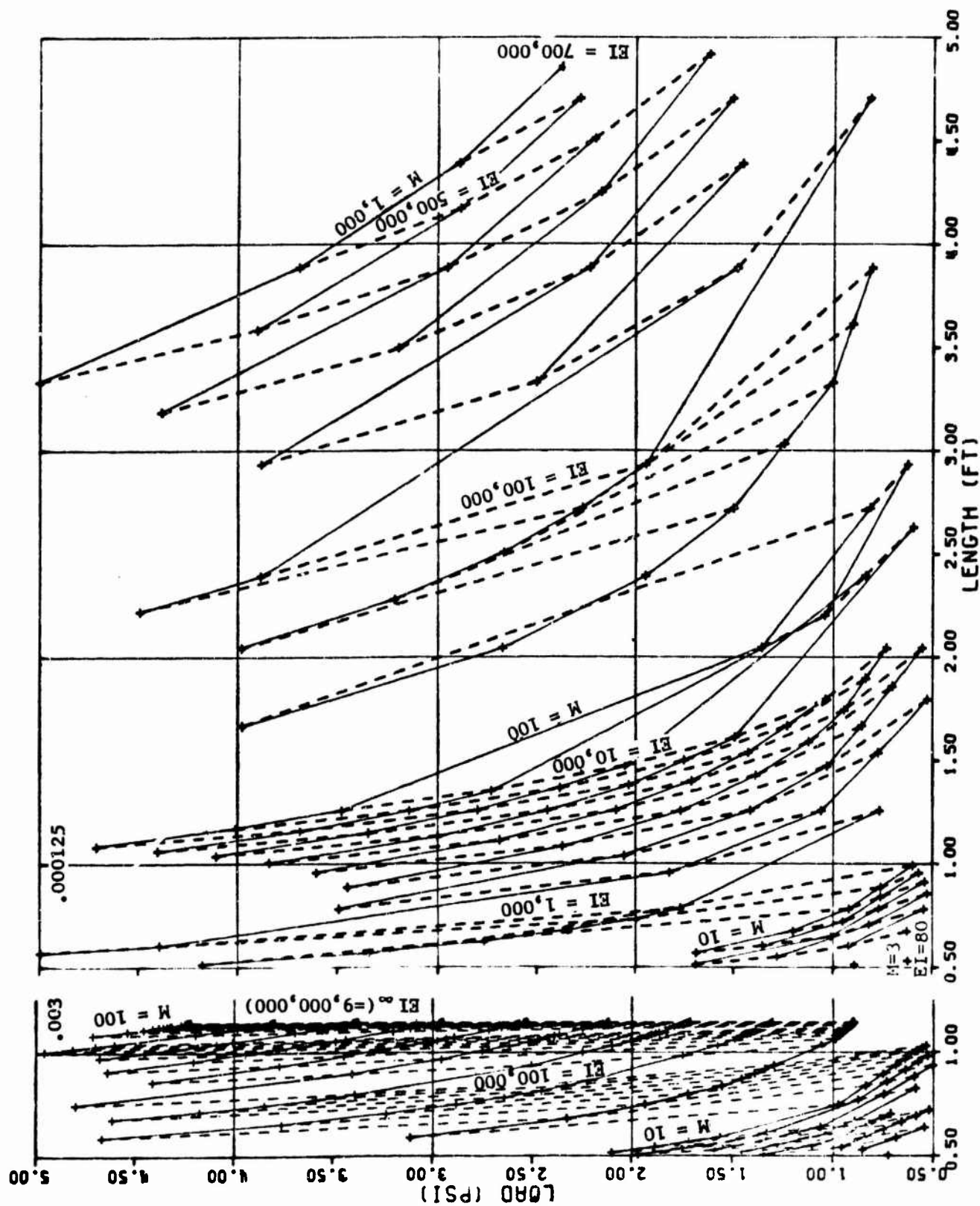
Fig. 6 Constant creep condition and deflection criterion at different attachments.



deflection criteria: 50% of "one" and "two"  
creep condition:  $.003 \text{ in}^{-1}$   
attachment: clamped-clamped support

Fig. 7 Constant creep condition and attachments at different deflection criteria.





deflection criterion: 50% of "one"  
 creep conditions: .003 and .000125 in<sup>-1</sup>  
 attachment: free-free support

Fig. 8 Constant deflection criterion and attachments at different creep conditions.

load (psi)

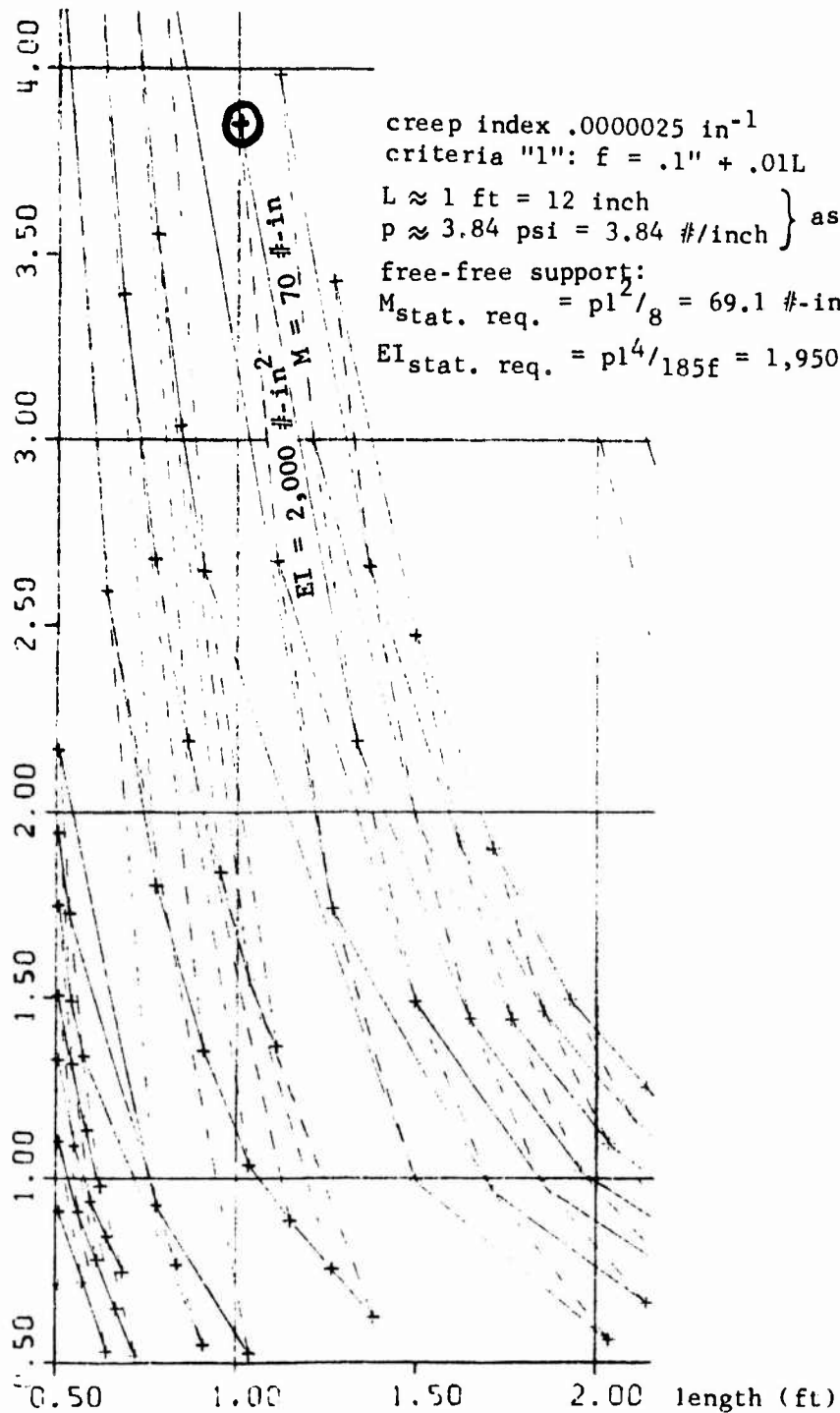


Fig. 9 Quasi-elastic case at low creep index.

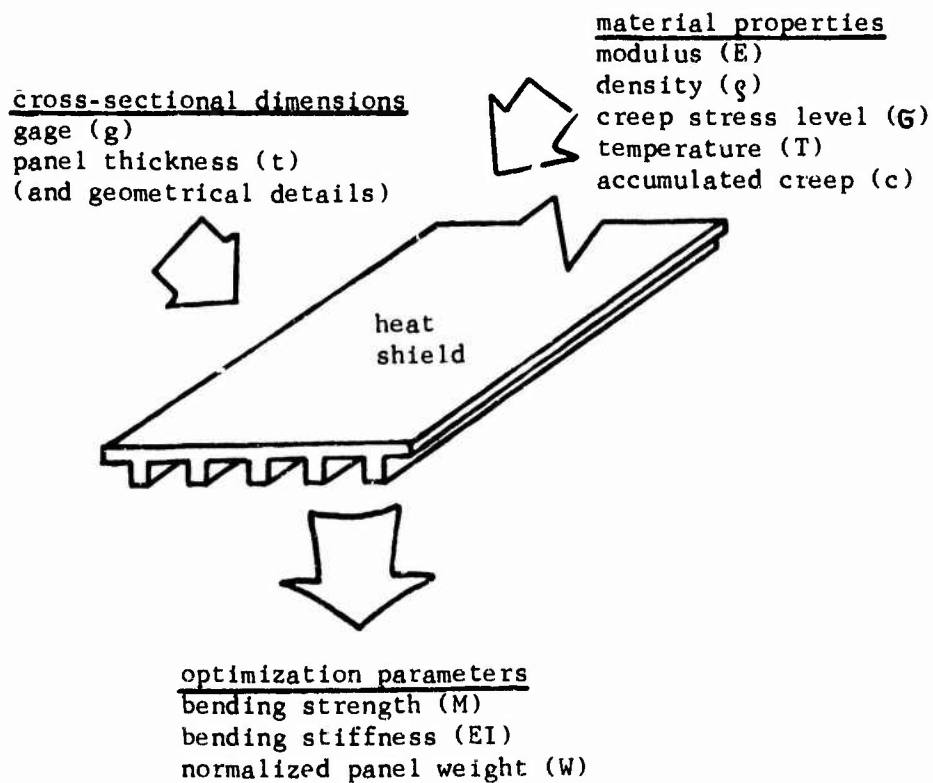


Fig. 10 Materials concepts and assessment algorithm "2".

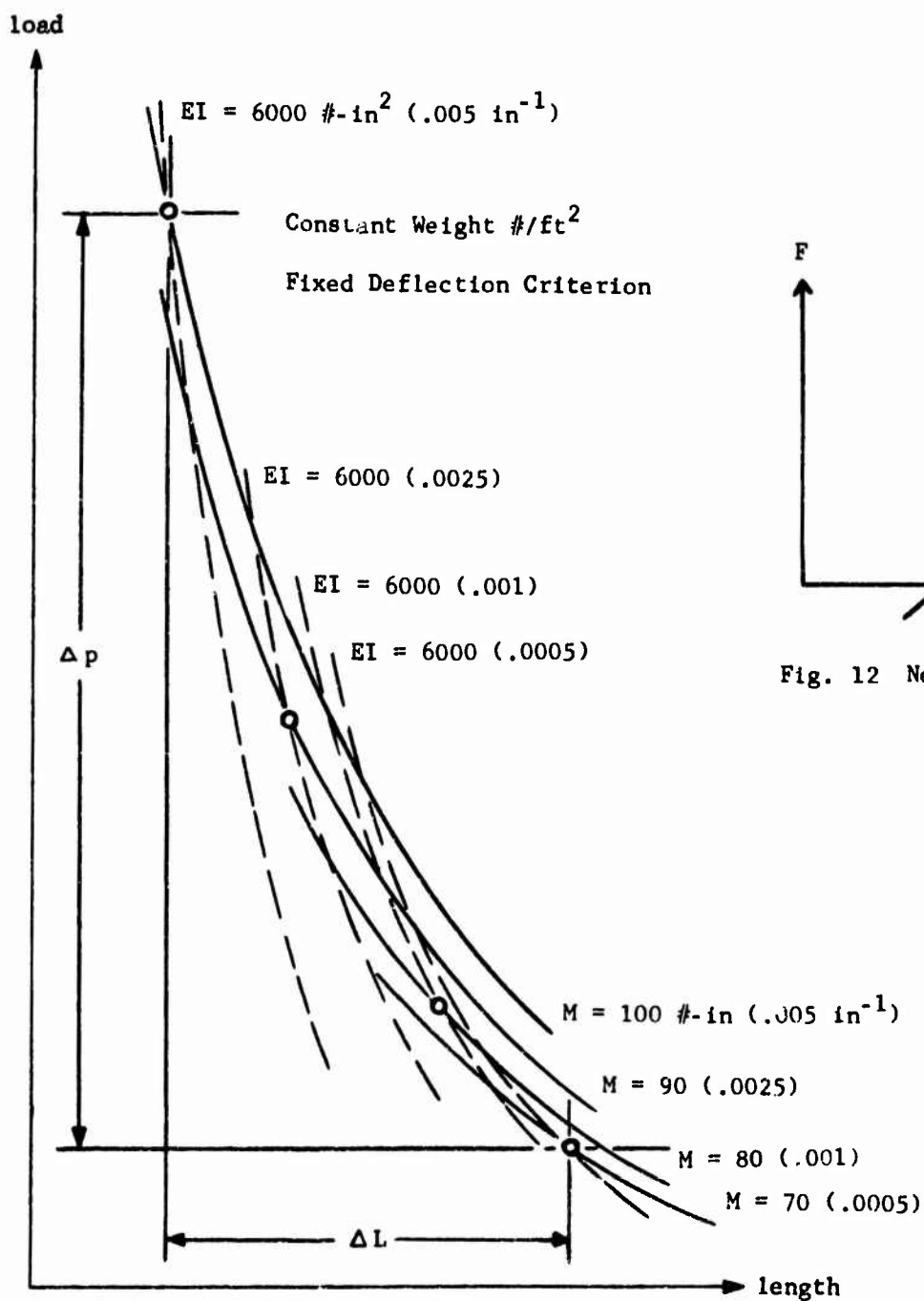


Fig. 11 Creep index trade-off.

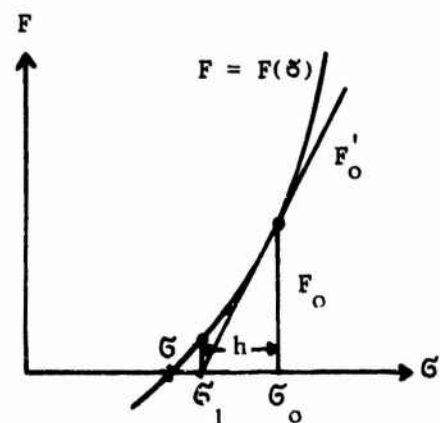


Fig. 12 Newton's interpolation.

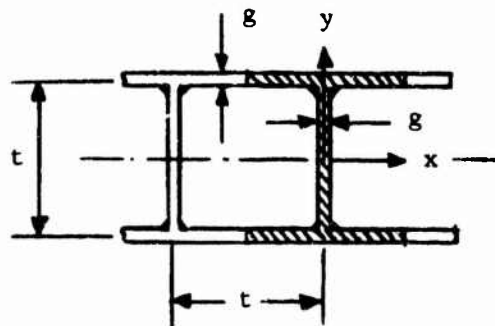


Fig. 13 Square channel cross section.

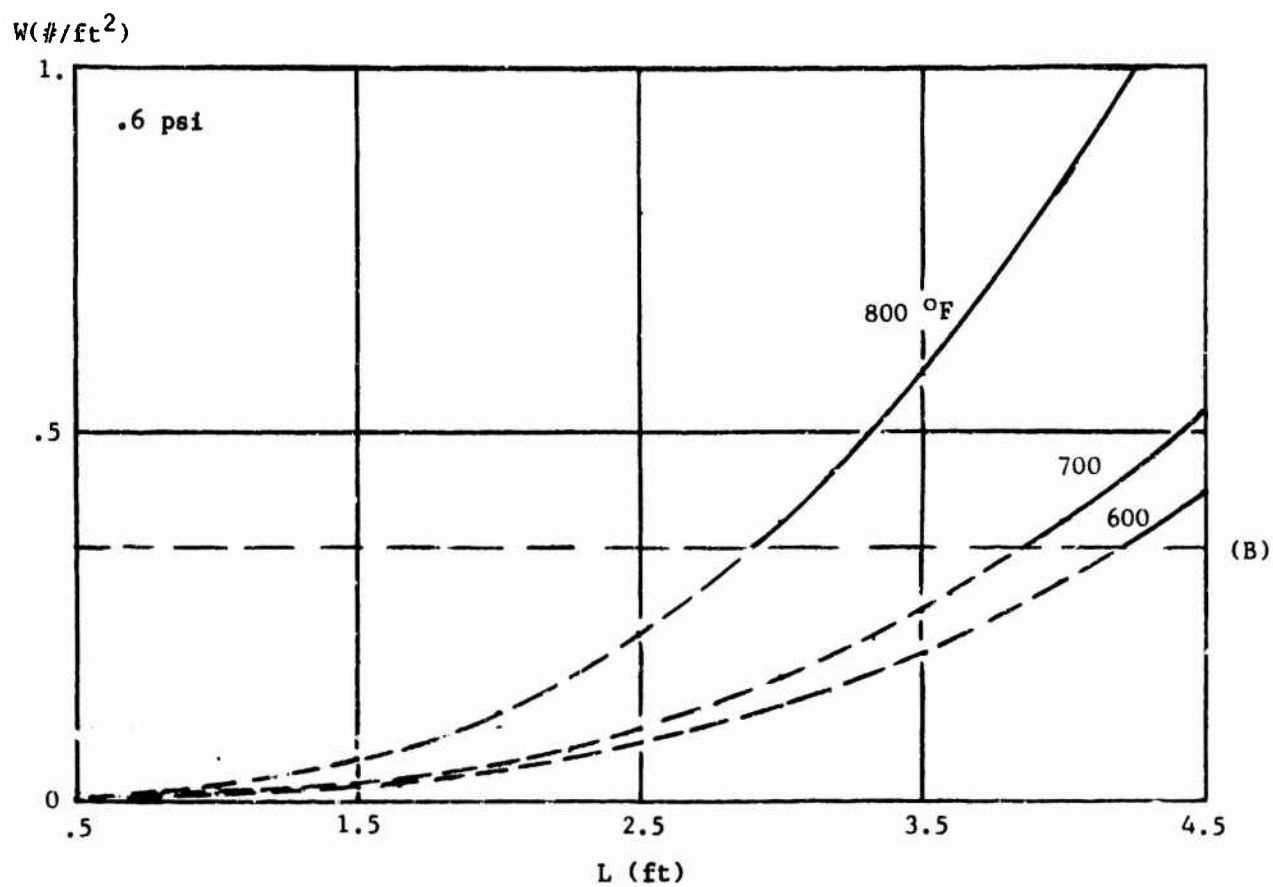


Fig. 14 Net panel weights at different temperatures (fixed panel depth).

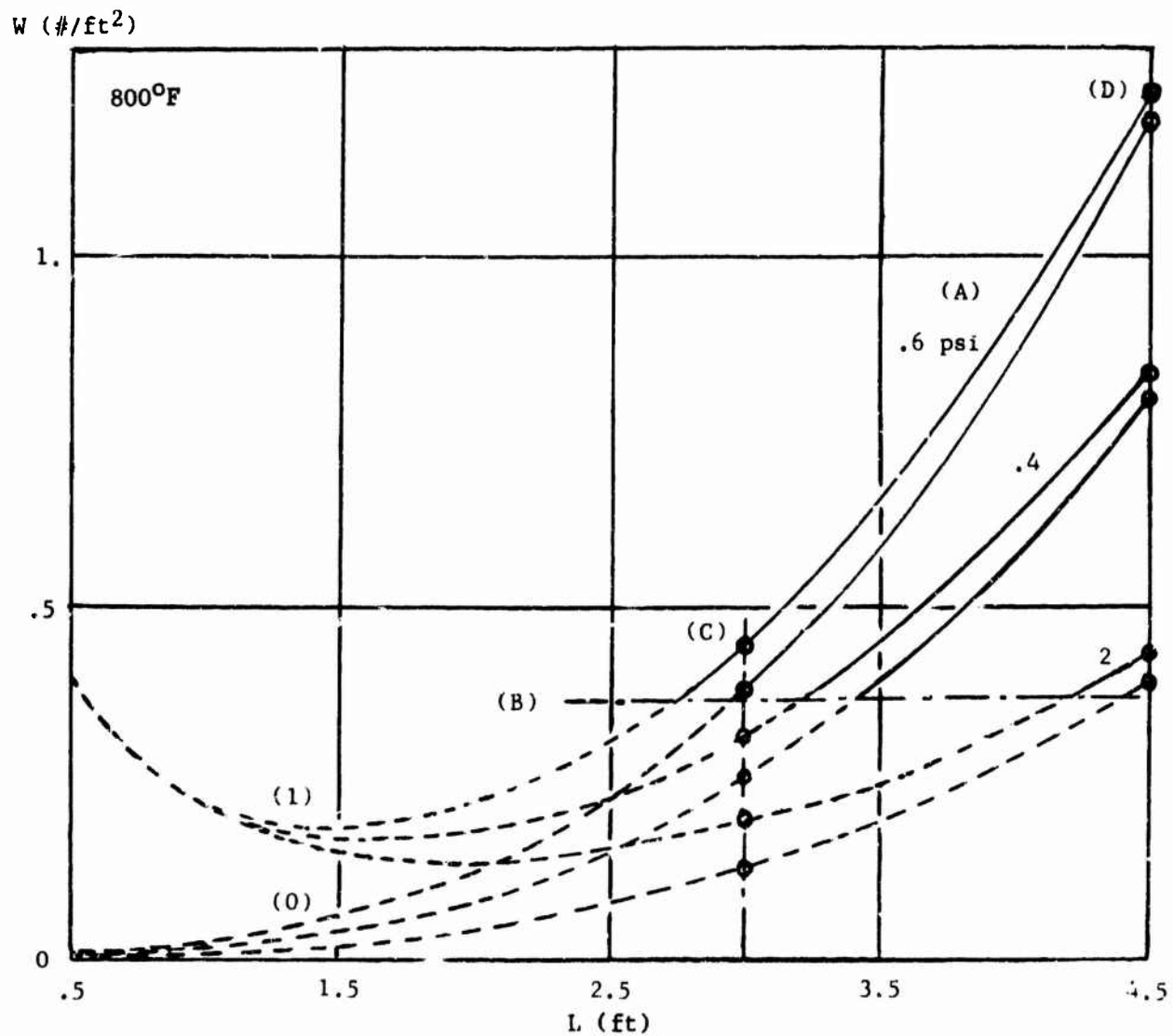


Fig. 15 Net and support weights vs. panel length.

individual scale  
(dimension)

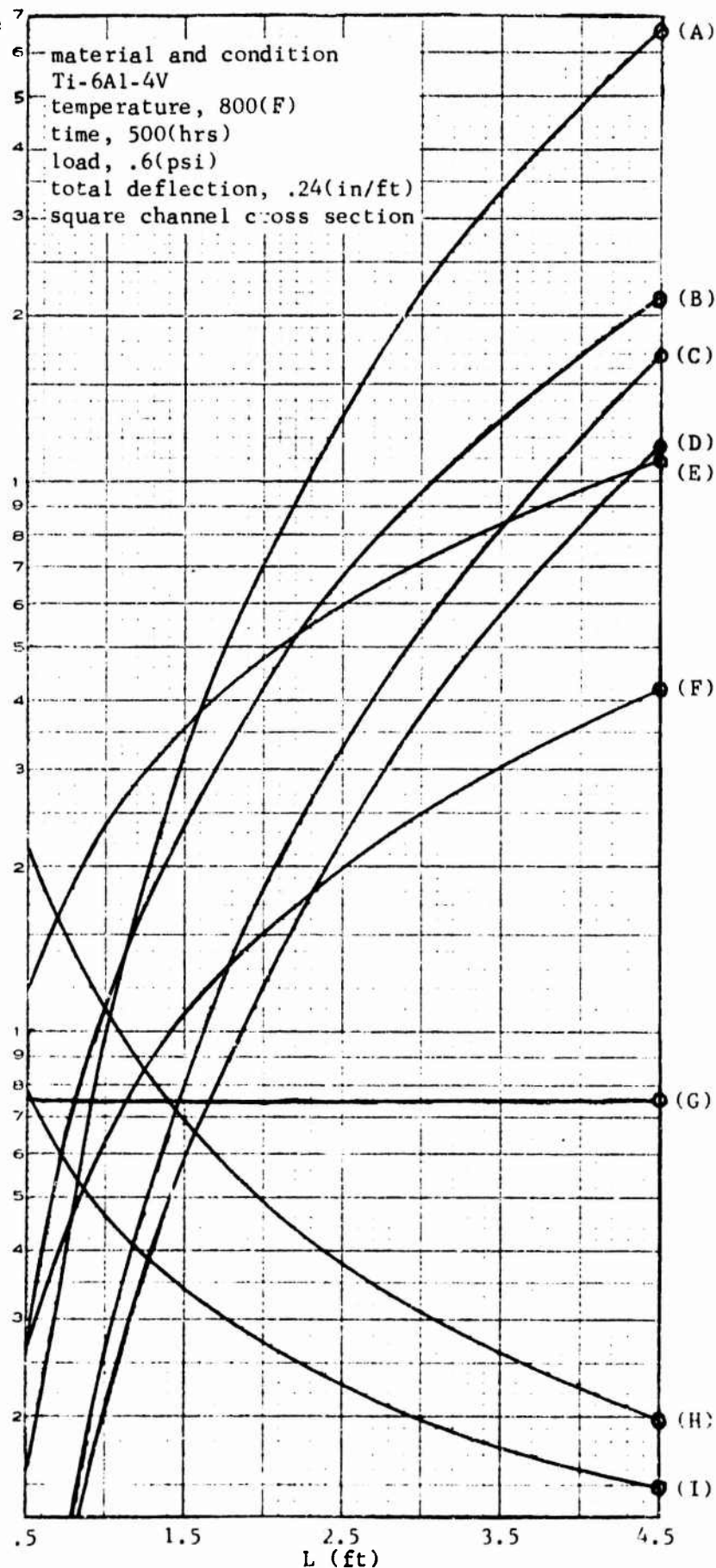


Fig. 16 Variational trends of properties at constant panel depth.

individual scale  
(dimension)

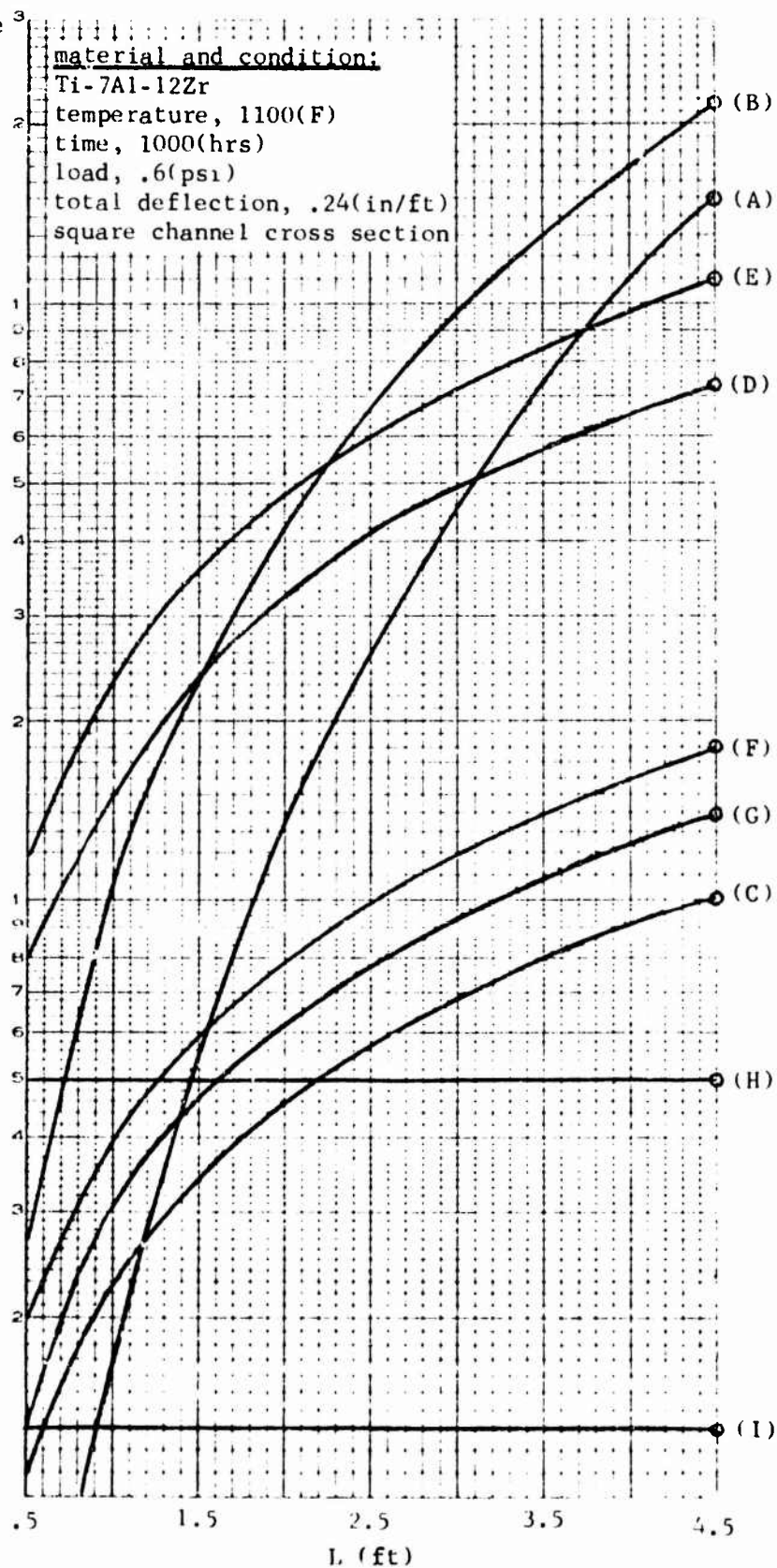


Fig. 17 Variational trends of properties at constant creep and stress level.



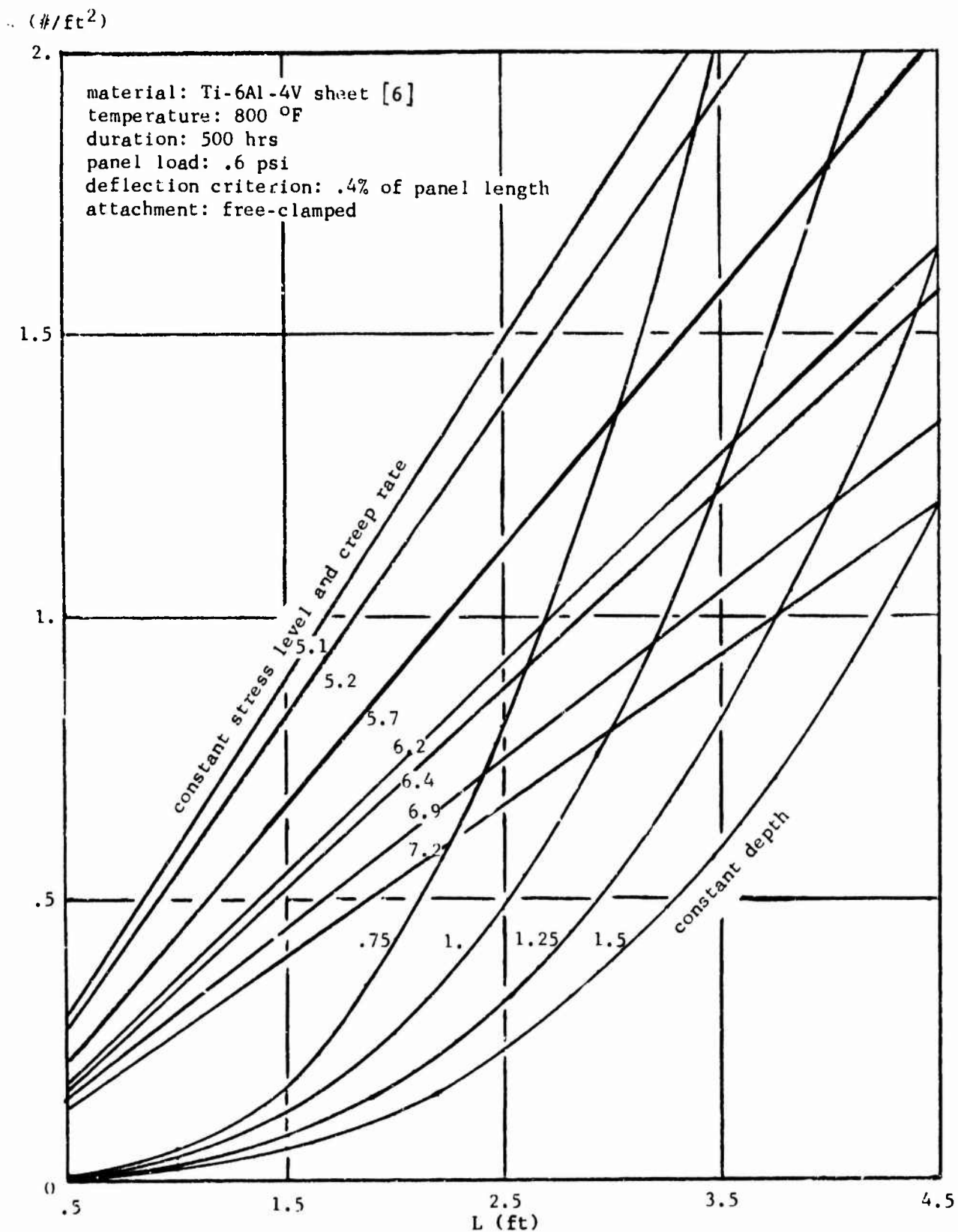


Fig. 18 Weight vs. panel length, comparison of constant stress and creep and constant panel depth.

weight  
#/sqft

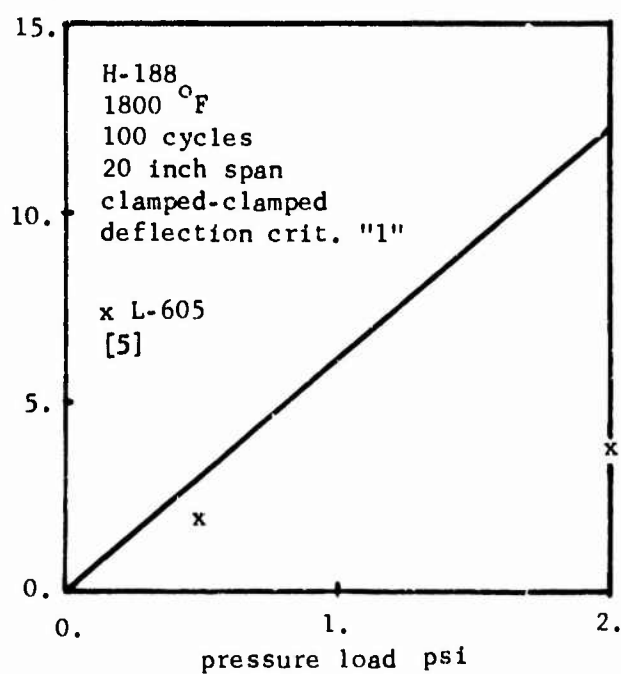


Fig. 19 Comparison of TPS weights.

$M_\infty$	alt. [ft]	$T_A$ [°F]	$T_s$ [°F]
2.3	75,000	295	355
3.0	75,000	550	650
5.0	120,000	1850	1150

Tab. 1 Adiabatic wall and stagnation temperature [1].

support	free-free	free-clamped	clamped-clamped
$c_1$	.125	.125	.0833
$c_2$	.2078	.08649	.00625
$c_3$	.01302	.003405	.002604

Tab. 2 Elastic boundary constants.

total deflection [in]	100%	50%	20%
criterion "one"	.1" + .12 * L	.05" + .06 * L	.02" + .024 * L
criterion "two"	.24 * L	.12 * L	.048 * L

(L = length in ft)

Tab. 3 Criteria of total deflection.

temperature [°F]	max. stress [ksi]	scatter of creep data [in/in]		handbook data [in/in]
		static	cyclic	
300	40	.0061-.0131	.0038-.0053	.005
350	14	.0017-.0031	.0007-.0021	.002
500	18	.0047-.0058	.0078-.011	.005

Tab. 4 Creep data for 2219-T87 aluminum [12].

temp. [°F]	time [hr]	stress [ksi]	alloy	ref.
900	100	77	AF-1	[25]
		74	RMI 5621-S( $\beta$ -forged)	"
		13	Ti-6-4	[26]
	1000	72	AF-1	[25]
		66.5	RMI 5621-S( $\beta$ -forged)	"
		66.5	AF-2, Ti-77	"
1000	100	65.5	AF-1	"
		60	RMI 5621-S( $\beta$ -forged)	"
		57	RMI 5621-S( $\alpha\beta$ -forged)	"
		55	AF-2, Ti-77	"
		13	Ti-8Al-2Cb-1Ta	[10]
	1000	44	AF-1	[25]
		30	RMI 5621-S( $\beta$ -forged)	"
		9	Ti-8Al-2Cb-1Ta	[10]

Tab. 5 Creep strength (.2%) of titanium alloys.

	static conditions	constant temp/ cyclic stress	constant stress/ cyclic temp.	cyclic conditions
number of tests	9	3	2	9
scatter of creep data in/in	.0011-.0029	.0028-.0039	.0059-.0072	.0043-.0068
average creep in/in	.0021	.0034	.0065	.0058

Tab. 6 Creep data for T1-6-4 (STA) [12].

material	load [psi] or type of design	max. temp. [°F]	unit weight [#/ft <sup>2</sup> ]
T1	MSFC	600	1.05
T1	.5	800	.72
T1	2.	800	.75
T1	Phase B	850	.8
Ré 41	MSFC	1300	1.95
L-605	MSFC	1575	3.7
Ré 41	.5	1600	1.1
Ré 41	2.	1600	1.8
Ré 41	Phase B	1600	1.
L-605	.5	1800	1.9
L-605	Phase B	1800	3.65
L-605	2.	1800	3.85
Cb	Phase B	2200	2.2
Cb	.5	2400	2.4
Cb	2.	2400	4.05

Tab. 7 Metallic heat shield weights at temperature [5].

Material	°F	ksi	elongation % predicted	elongation % actual	Remarks: Environmental shuttle conditions; 50 cycles of simultaneous temperature and heat
René 41					Considered up to 1600°F
	1600	8.5	1.6	21.3	Heat treatment, 1400°F age; scatter of actual elongation from 20 to 23%
	1600	8.5	.06	.8	2050°F solution treated, 1650°F age; scatter of actual elongation from .45 to 1.35%; 38% reduction to 110 ksi of $F_{tu}$ at R.T.
TD Ni-Cr	1800	2.	.08	.79	
					Considered to 2200°F; actual and predicted creeps considerably low, almost identical
	1800	6.5	.06	.264	4% reduction to 115% of $F_{tu}$ at R.T.
	2000	5.	.098	.124	
H 188	2200	3.5	.13	.106	Actual and predicted creep are reversed
					Considered to 1800°F; for .008" sheet: Low oxida- tion at 1800°F, 50 hrs cycled, .3 mils per side [4]
	1800	2.	.25	.59	
Hast X	1800	5.	5.3	7.9	58% reduction to 55 ksi of $F_{tu}$ at R.T.
					High metal loss, 2.65 mils per side [4]
	1800	2.	1.1	2.9	

Tab. 8 Cyclic creep of superalloys [8].

max. temperature [°F]	temperature cycling		stress cycling	
	adequate	inadequate	adequate	inadequate
iron-base 12Cr5Mo	1050	1350	?	?
FeA-18Cr8Ni	1150	1550	1500	?
type 321 stainless	1200	1350	1500	?
Ni-Chr steel N155	?	1500	1500	?
iron-base A-286	1400	?	?	?

Tab. 9 Maximum temperatures for separate stress cyclic and temperature cyclic prediction [14].

.016"	integrally stiffened skin
.010"	flat skin
.010"	single corrugation
.008"	skin plus corrugation skin
.008"	sandwich facings
.002"	sandwich corrugations

Tab. 10 Minimum gages for L-605, McDonnell data.

panel weight	1.25 [#/ft <sup>2</sup> ]
R.T. ult. bending strength	147 [#-in/in]
dimensions:	
gag. thickness	.008" (.008") <sup>x</sup>
panel depth	.29" (.5"+.1" bead effect)
hat distance	1.2" (1.)
hat size at top	1." (.7")
hat size at bottom	.85" (.5")
<sup>x</sup> panel No. 2 data [8] in parentheses	

Tab. 11 Design data for L-605 heat shield [7].

manufacturer/ evaluator	ref.	composition of coating	Ta-alloy/ substrate	oxidation environment	max. temp. [°F]	time [hr]/ $\frac{1}{2}$ hr cycle to failure	max. temp. time [hr] [°F] to failure
Solar	[32]	Si-20Fe-10Mo-5Ti-5V	Ta-10W	10 torr	2600	80 <sup>+</sup> cyc	
Lockheed		Si-20Mn-27Ti				50-100 <sup>+</sup> cyc	
		Si-33Co-22Mo				59-100 <sup>+</sup> cyc	
		Si-20Ti-10Mo(512C)				8, 10 cyc	
Sylvania							
TRW	[42]	W Si <sub>2</sub>	arc cast W substrate	atm. static air	3200	13 hrs.	3500 2 hrs
		W/W Si <sub>2</sub>	Ta-10W			12 hrs.	3600 nil
Vitro		W+Ti/W Si <sub>2</sub>	T-222			3½ hrs.	3400 1 hr.

Tab. 12 Performance of oxidation protective tantalum alloy coatings.

Unit Weight lb/ft <sup>2</sup> of concepts	12 inch span		24 inch span	
	Short time	Creep Criteria	Short time	Creep Criteria
honeycomb	4.1	4.8	4.9	7.8
rib stiffened	4.9	5.8	6.6	12.
single faced V shaped	5.5	6.	7.5	13.8
single faced flat corrugated	6.	6.5	8.	12.2

Tab. 13 Weight penalties of coated T-222 TPS designed for creep [15].



# APPENDIX

```

DIMENSION B(4),C1(18),C2(18),C3(18),P(5),PF(5),L(10),C(5,10),
1D(5,10),EI(5,10),F(5,10),G(5,10),I(5,10),M(5,10),S(5,10),ST(5,10),
2W(5,10,4)
REAL I,L,M
C1(1)=.125
C2(1)=.2078
C3(1)=.01302
C1(2)=C1(1)
C2(2)=.08649
C3(2)=.005405
C1(3)=.0833
C2(3)=.00625
C3(3)=.002604
DO 100 KK1=1,5
KK2=3*KK1
C1(KK2+1)=C1(1)
C2(KK2+1)=C2(1)
C3(KK2+1)=C3(1)
C1(KK2+2)=C1(2)
C2(KK2+2)=C2(2)
C3(KK2+2)=C3(2)
C1(KK2+3)=C1(3)
C2(KK2+3)=C2(3)
100 C3(KK2+3)=C3(3)
180 READ (5,105) TITLE,TEMP,TIME,R,T,E,KK,JP,KL,NN,B
IF (EOF(5)) 110,115
105 FORMAT (A4,5E8.2,I2,3I1,4F3.1)
CREEP EQ. FOR TI-6AL-4V (MIL-HDBK-5A)
115 TE=TEMP+450.
T1=TE-917.
T2=TE-975.
T3=TE-1047.
A1=2758./T1
A2=105.8/T2
A3=3.759/T3
B1=.0225-A1
B2=.0159+A2
B3=-.924-A3
C01=EXP(B1)
C02=EXP(B2)
C03=EXP(B3)
C03=TIME**C03
C01=.01*C01*C03
C03=C02-1.
TLMC=.555*(TEMP-32.)
P(1)=.2
P(1)=1.
PF(1)=28.8
PF(1)=1+.
DO 120 J=2,JP
P(J)=P(J-1)+.2
P(J)=P(J-1)+1.
120 PF(J)=P(J)*144.
L(1)=.5

```

```

      DO 125 K=2,KL
125  L(K)=L(K-1)+.5
      DO 130 J=1,JP
      DO 135 K=1,KL
C BENDING STRENGTH REQUIRED
      M(J,K)=C1(KK)*P(J)*(L(K)*12.)**2
      GO TO (1,1,1,2,2,2,3,3,3,4,4,4,5,5,5,6,6,6)KK
C TOTAL ALLOWABLE DEFLECTION
      1 D(J,K)=.1+.12*L(K)
      GO TO 140
      2 D(J,K)=.24*L(K)
      GO TO 140
      3 D(J,K)=.05+.06*L(K)
      GO TO 140
      4 D(J,K)=.12*L(K)
      GO TO 140
      5 D(J,K)=.02+.024*L(K)
      GO TO 140
      6 D(J,K)=.048*L(K)
C TOTAL STRAIN
      140 ST(J,K)=D(J,K)*T/(C2(KK)*(L(K)*12.)**2)
C STRESS LEVEL AND CREEP INTERPOLATION (NEWTON)
      X0=ST(J,K)*E/1000.
      DO 145 JJ=1,100
      Y0=C01*X0**C02+X0*1000./E-ST(J,K)
      YP=C01*C02*X0**C03+1000./E
      X1=X0-Y0/YP
      DX=X1-X0
      DX=ABS(DX)
      IF (DX .LE. .01) GO TO 150
      X0=X1
145  CONTINUE
150  S(J,K)=X1
      C(J,K)=C01*X1**C02
C MOMENT OF INERTIA
      I(J,K)=.0005*M(J,K)*T/S(J,K)
C GAGE THICKNESS (SQUARE CHANNEL CROSS SECTION)
      G(J,K)=1.714*I(J,K)/T**2
C BENDING STIFFNESS AND ELASTIC DEFLECTION
      EI(J,K)=I(J,K)*E
      F(J,K)=C3(KK)*P(J)*(L(K)*12.)**4/EI(J,K)
C PANEL WEIGHT (NET AND WITH SUPPORTS)
      W(J,K,1)=432.*G(J,K)*R
      DO 155 N=1,NN
155  W(J,K,N)=W(J,K,1)+B(N)/L(K)
135  CONTINUE
130  CONTINUE
      WRITE (6,160)
160  FORMAT (/132H TEMPERATURE TIME MATL SPZWT ALWST ELMOD CREEP
122ES.LOAD SIZE FX TOTDPL ELDEFL "M" "I" "EI" OPT4 GA
23E SUPW WGHT/132H DEG.F DEG.C HPS. SYST LB/CI KSI PSI IN.
3/IN. PSF PSI FT CR IN. IN. LB-IN IN**4 LB-SQI IN
4. IN. LB/F L/S+)
      DO 165 N=1,NN
      DO 170 J=1,JP

```

```

WRITE (6,175) (TEMP,TLMC,TIME,TITLE,R,S(J,K),E,C(J,K),PF(J),P(J),
1L(K),KK,J(J,K),F(J,K),M(J,K),I(J,K),EI(J,K),T,G(J,K),B(N),
2W(J,K,N),K=1,KL)
175 FORMAT (1X,F5.0,2F6.0,1X,A4,F4.2,3E8.2,F5.0,2F5.2,1X,I2,5E8.2,
1F5.2,E8.2,2F5.2)
170 CCNTINUE
165 CONTINUE
GO TO 130
110 STOP
END

```

TEMPERATURE DEG.F	TIME DEG.C	MATL HRS.	SPZWT SYST	ALWST LB/CI	ELMOD KSI	CREEP PSI	PRES. IN./IN.	LOAD PSF	SIZE PSI	FT
800.	426.	500.	TI64	.16	.95E+02	.12E+08	.31E-01	144.	1.00	.50
800.	426.	500.	TI64	.16	.57E+02	.12E+08	.14E-01	144.	1.00	1.00
800.	426.	500.	TI64	.16	.43E+02	.12E+08	.93E-02	144.	1.00	1.50
800.	426.	500.	TI64	.16	.34E+02	.12E+08	.68E-02	144.	1.00	2.00
800.	426.	500.	TI64	.16	.29E+02	.12E+08	.53E-02	144.	1.00	2.50
800.	426.	500.	TI64	.16	.25E+02	.12E+08	.43E-02	144.	1.00	3.00
800.	426.	500.	TI64	.16	.22E+02	.12E+08	.36E-02	144.	1.00	3.50
800.	426.	500.	TI64	.16	.20E+02	.12E+08	.31E-02	144.	1.00	4.00
800.	426.	500.	TI64	.16	.19E+02	.12E+08	.27E-02	144.	1.00	4.50

FX	TOTDFL IN.	ELDEFL IN.	"M" LB-IN	"I" IN**4	"EI" LB-SQI	DPTH IN.	GAGE IN.	SUPW LB/P	WGHT L/SF
5	.12E+00	.25E-01	.45E+01	.24E-04	.28E+03	1.00	.40E-04	0.00	.00
5	.24E+00	.60E-01	.18E+02	.16E-03	.19E+04	1.00	.27E-03	0.00	.02
5	.36E+00	.99E-01	.40E+02	.48E-03	.57E+04	1.00	.82E-03	0.00	.06
5	.48E+00	.14E+00	.72E+02	.10E-02	.13E+05	1.00	.18E-02	0.00	.12
5	.60E+00	.19E+00	.11E+03	.19E-02	.23E+05	1.00	.33E-02	0.00	.23
5	.72E+00	.24E+00	.16E+03	.32E-02	.38E+05	1.00	.55E-02	0.00	.38
5	.84E+00	.29E+00	.22E+03	.49E-02	.59E+05	1.00	.84E-02	0.00	.58
5	.96E+00	.34E+00	.29E+03	.71E-02	.85E+05	1.00	.12E-01	0.00	.84
5	.11E+01	.39E+00	.36E+03	.98E-02	.12E+06	1.00	.17E-01	0.00	1.17

```

      INTEGER P
      REAL M
      COMMON DATA(603)
      COMMON /BLK1/ CRRATE, TIME, HGHT, P(72), EJ(72), PRLOA2(10)
      COMMON /BLK2/ DFMA(4,10,3)
      COMMON /BLK3/ ZP(4,3)
      COMMON /BLK4/ X(700,6,2), Y(700,6,2)
      COMMON /BLK5/ NN(6,2)
      COMMON /BLK6/ NNN(72,6,2)
      DIMENSION NNPREV(6)
      CALL PLOTS (DATA,603)
      M(1)=.01
      DO 100 I=2,9
100  M(I)=M(I-1)+.01
      DO 105 I=1,7
      DO 110 J=1,9
      K=9*(I-1)+J
      K1=9*I+J
110  M(K1)=M(K)*10.
105  CONTINUE
      EJ(1)=1.
      DO 115 J=2,9
115  EJ(J)=EJ(J-1)+1.
      DO 120 I=1,7
      DO 125 J=1,9
      K=9*(I-1)+J
      K1=9*I+J
125  EJ(K1)=EJ(K)*10.
120  CONTINUE
      PRLOA2(1)=.5
      DO 130 P=2,10
130  PRLOA2(P)=.5+PRLOA2(P-1)
220  READ (5,135) CRRATE, TIME, HGHT, KENDFL
135  FORMAT (3E8.2, I1)
      WRITE (6,140) CRRATE, TIME, HGHT
140  FORMAT (1H1, 3(3X, E8.2))
      HGHT=HGHT*.5
      DO 145 K=1,2
      DO 150 N=1,6
      DO 155 I=1,72
155  NNN(I,N,K)=0
150  CONTINUE
145  CONTINUE
      DO 160 K=1,2
      DO 165 N=1,6
165  NN(N,K)=0
      IF (K.EQ. 2) GO TO 170
      DO 175 I=1,72
      DO 180 N=1,6
180  NNPREV(N)=NN(N,K)
      DO 185 J=1,72
      CALL ELAPL (I,J)
      CALL ZERMA (K)
185  CONTINUE
      DO 190 N=1,6

```

```

190 NNN(I,N,K)=NN(N,K)-NIPRIV(N)
175 CONTINUE
    IF (K.EQ. 1) GO TO 160
170 DO 195 J=1,72
    DO 200 N=1,6
200 NIPRIV(N)=NN(N,K)
    DO 215 I=1,72
    CALL ELAFL (I,J)
    CALL ZIRMA (K)
205 CONTINUE
    DO 210 N=1,6
210 NNN(J,N,K)=NN(N,K)-NIPRIV(N)
195 CONTINUE
160 CONTINUE
    CALL GRPH
    IF (KENDPL .NE. 1) GO TO 215
    CALL PLOT
215 GO TO 220
END

```

```

SUBROUTINE ELAFL (I,J)
INTEGER P
REAL M, LENG1, LENG2
COMMON /BLK1/ CRRATE, TIME, HGHT, M(72), EJ(72), PRLCA2(10)
COMMON /BLK2/ CFMA(4, 10, 3)
DIMENSION LENG1(10), PRLCA1(10, 3), ELADF1(10, 3), PLADF1(10, 3),
1TOTCF1(10, 3), DFCR11(10), DFCR21(10), LENG2(10, 3), ELADF2(10, 3),
2PLADF2(10, 3), TOTCF2(10, 3), DFCR12(10, 3), DFCR22(10, 3)
LENG1(1)=.5
DO 100 L=2,10
100 LENG1(L)=.5+LENG1(L-1)
DO 105 L=1,10
C OTHER DEFLECTION CRITERION
DFCR11(L)=.1+.12*LENG1(L)
DFCR11(L)=.2*DFCR11(L)
DFCR21(L)=.24*LENG1(L)
105 DFCR21(L)=.2*DFCR21(L)
DO 110 L=1,10
PRLCA1(L,1)=8.*M(I)/(LENG1(L)*12.)**2
ELADF1(L,1)=.01302083*PRLCA1(L,1)*(LENG1(L)*12.)**4/EJ(J)
PLADF1(L,1)=.10416667*CRRATE*TIME*(LENG1(L)*12.)**2/HGHT
TOTCF1(L,1)=ELADF1(L,1)+PLADF1(L,1)
CFMA(1,L,1)=1.-TOTCF1(L,1)/DFCR11(L)
110 CFMA(2,L,1)=1.-TOTCF1(L,1)/DFCR21(L)
DO 115 L=1,10
PRLCA1(L,2)=PRLCA1(L,1)
ELADF1(L,2)=.0054054*PRLCA1(L,2)*(LENG1(L)*12.)**4/EJ(J)
PLADF1(L,2)=.0432432*CRRATE*TIME*(LENG1(L)*12.)**2/HGHT
TOTCF1(L,2)=ELADF1(L,2)+PLADF1(L,2)
CFMA(1,L,2)=1.-TOTCF1(L,2)/DFCR11(L)
115 CFMA(2,L,2)=1.-TOTCF1(L,2)/DFCR21(L)
DO 120 L=1,10
PRLCA1(L,3)=PRLCA1(L,1)*1.5
PLADF1(L,3)=.00260417*PRLCA1(L,3)*(LENG1(L)*12.)**4/EJ(J)
PLADF1(L,3)=.03125*CRRATE*TIME*(LENG1(L)*12.)**2/HGHT

```

```

      TOTCF1(L,3)=FLADF1(L,3)+PLADF1(L,3)
      CFMA(1,L,3)=1.-TCTDF1(L,3)/DFCR11(L)
120  CFMA(2,L,3)=1.-TCTDF1(L,3)/DFCR21(L)
      DO 125 P=1,10
      LENG2(P,1)=A.*M(I)/PRLGA2(P)
      LENG2(P,1)=SQRT(LENG2(P,1))
C  OTHER DEFLECTION CRITERION
      DFCR12(P,1)=.1+.01*LENG2(P,1)
      DFCR12(P,1)=.2*DFCR12(P,1)
      DFCR22(P,1)=.02*LENG2(P,1)
      DFCR22(P,1)=.2*DFCR22(P,1)
      ELADF2(P,1)=.01302033*PRLGA2(P)*LENG2(P,1)**4/EJ(J)
      FLADF2(P,1)=.10416667*CRRATE*TIME*LENG2(P,1)**2/HGHT
      TOTCF2(P,1)=ELADF2(P,1)+FLADF2(P,1)
      CFMA(3,P,1)=1.-TCTDF2(P,1)/DFCR12(P,1)
125  CFMA(4,P,1)=1.-TOTDF2(P,1)/DFCR22(P,1)
      DO 130 P=1,10
      LENG2(P,2)=LENG2(P,1)
C  OTHER DEFLECTION CRITERION
      DFCR12(P,2)=.1+.01*LENG2(P,2)
      DFCR12(P,2)=.2*DFCR12(P,2)
      DFCR22(P,2)=.02*LENG2(P,2)
      DFCR22(P,2)=.2*DFCR22(P,2)
      ELADF2(P,2)=.00540540*PRLGA2(P)*LENG2(P,2)**4/EJ(J)
      FLADF2(P,2)=.0432432*CRRATE*TIME*LENG2(P,2)**2/HGHT
      TOTCF2(P,2)=ELADF2(P,2)+FLADF2(P,2)
      CFMA(3,P,2)=1.-TCTDF2(P,2)/DFCR12(P,2)
130  CFMA(4,P,2)=1.-TOTDF2(P,2)/DFCR22(P,2)
      DO 135 P=1,10
      LENG2(P,3)=12.*M(I)/PRLGA2(P)
      LENG2(P,3)=SQRT(LENG2(P,3))
C  OTHER DEFLECTION CRITERION
      DFCR12(P,3)=.1+.01*LENG2(P,3)
      DFCR12(P,3)=.2*DFCR12(P,3)
      DFCR22(P,3)=.02*LENG2(P,3)
      DFCR22(P,3)=.2*DFCR22(P,3)
      ELADF2(P,3)=.00260417*PRLGA2(P)*LENG2(P,3)**4/EJ(J)
      FLADF2(P,3)=.03125*CRRATE*TIME*LENG2(P,3)**2/HGHT
      TOTCF2(P,3)=ELADF2(P,3)+FLADF2(P,3)
      CFMA(3,P,3)=1.-TOTDF2(P,3)/DFCR12(P,3)
135  CFMA(4,P,3)=1.-TOTDF2(P,3)/DFCR22(P,3)
      RETURN
      END

      SUBROUTINE ZERMA (K)
      COMMON /BLK2/ CFMA(4,10,3)
      COMMON /BLK3/ ZM(4,3)
      COMMON /BLK4/ X(700,2),Y(700,6,2)
      COMMON /BLK5/ NN(6,2)
      DO 100 II=1,4
      DO 105 JJ=1,3
105  ZM(II,JJ)=0.
100  CONTINUE
      DO 110 II=1,4
      DO 115 JJ=1,3

```

```

      IF (DFMA(II,1,JJ) .LT. .0) GO TO 120
      DO 125 KK=2,10
      IF (DFMA(II,KK,JJ) .LT. .0) GO TO 130
125  CONTINUE
      GO TO 115
130  ZM(II,JJ)=.5*FLOAT(KK-1)+.5*DFMA(II,KK-1,JJ)/(DFMA(II,KK-1,JJ)
      1-DFMA(II,KK,JJ))
      GO TO 115
120  DO 135 KK=2,10
      IF (DFMA(II,KK,JJ) .GT. .0) GO TO 140
135  CONTINUE
      GO TO 115
140  ZM(II,JJ)=.5*FLOAT(KK-1)-.5*DFMA(II,KK-1,JJ)/(DFMA(II,KK-1,JJ)
      1-DFMA(II,KK,JJ))
115  CONTINUE
110  CONTINUE
      DO 145 II=1,2
      DO 150 JJ=1,3
      N=(II-1)*3+JJ
      IF (ZM(II,JJ)*ZM(II+2,JJ)) 150,150,160
160  NN(N,K)=NN(N,K)+1
      KK=NN(N,K)
      X(KK,N,K)=ZM(II,JJ)
      Y(KK,N,K)=ZM(II+2,JJ)
150  CONTINUE
145  CONTINUE
      RETURN
      END

```

---

# SUBROUTINE GRPH

```

COMMON DATA(603)

```

```

COMMON /BLK4/ X(700,5,2),Y(700,6,2)

```

```

COMMON /BLK6/ NNA(72,6,2)

```

```

DIMENSION XX(72),YY(72)

```

```

DIMENSION BXAX(2),BYAX(2),BLA3(7),BL(6,7)

```

```

DATA BXAX(1)/12HLENGTH (FT) /,BYAX(1)/12H LOAD (PSI) /

```

```

DATA BL(1,1)/6H FREE-/ ,BL(1,2)/6HFREE S/,BL(1,3)/6HUPPCRT/

```

```

DATA BL(1,4)/6H / CR1/,BL(1,5)/6HEP DEF/,BL(1,6)/6HLCR1/

```

```

DATA BL(1,7)/6HT. 1 /,BL(2,1)/6HFREE-C/,BL(2,2)/6HLAMPED/

```

```

DATA BL(2,3)/6H SUPPD/,BL(2,4)/6HRT / C/,BL(2,5)/6HREEP D/

```

```

DATA BL(2,6)/6HFL. C/,BL(2,7)/6HRIT. 1/,BL(3,1)/6HCLAMPE/

```

```

DATA BL(3,2)/6HDC-CLAM/,BL(3,3)/6HPED SU/,BL(3,4)/6HP. / C/

```

```

DATA BL(4,7)/6HT. 2 /,BL(5,7)/6HRIT. 2/

```

```

C NUMBER OF PLOTS N=1,6

```

```

DO 100 N=1,6

```

```

CALL PLOT (0.,0.,-3)

```

```

CALL AXIS (0.,1.,BXAX,-12,9.,0.,.5,.5,10.)

```

```

CALL AXIS (0.,1.,BYAX,12,9.,90.,.5,.5,10.)

```

```

CALL PLOT (0.,2.,3)

```

```

CALL PLOT (9.,2.,2)

```

```

CALL PLOT (9.,4.,3)

```

```

CALL PLOT (0.,4.,2)

```

```

CALL PLOT (0.,6.,3)

```

```

CALL PLOT (9.,6.,2)

```

```

CALL PLOT (9.,8.,3)

```

```

CALL PLOT (0.,8.,2)
CALL PLOT (0.,10.,3)
CALL PLOT (9.,10.,2)
CALL PLOT (9.,1.,2)
CALL PLOT (7.,1.,3)
CALL PLOT (7.,10.,2)
CALL PLOT (5.,10.,3)
CALL PLOT (5.,1.,2)
CALL PLOT (3.,1.,3)
CALL PLOT (3.,10.,2)
CALL PLOT (1.,10.,3)
CALL PLOT (1.,1.,2)
CALL PLOT (0.,1.,-3)
CO 105 K=1,2
JSTART=0
CO 110 II=1,72
IF (NNN(II,N,K) .EQ. 0) GO TO 110
JNN=NNN(II,N,K)
CO 115 JJ=1,JNN
JJADD=JSTART+JJ
XX(JJ)=X(JJADD,N,K)
115 YY(JJ)=Y(JJADD,N,K)
XX(JNN+1)=.5
XX(JNN+2)=.5
YY(JNN+1)=.5
YY(JNN+2)=.5
JSTART=JSTART+JNN
IF (K .EQ. 2) GO TO 120
CALL LINE (XX,YY,JNN,1,1,3)
120 IF (K .EQ. 1) GO TO 110
CALL DASHLN (XX,YY,JIN,1)
110 CONTINUE
105 CONTINUE
CALL PLOT (0.,-1.,-3)
CO 125 KK=1,3
CO 130 LL=1,4
130 PL(KK+3,LL)=PL(KK,LL)
125 CONTINUE
CO 135 LL=5,6
PL(3,LL)=3L(2,LL)
PL(4,LL)=3L(1,LL)
PL(5,LL)=3L(2,LL)
135 EL(6,LL)=3L(2,LL)
PL(3,7)=3L(2,7)
EL(6,7)=EL(5,7)
CO 140 KK=1,7
140 ELAR(KK)=3L(N,KK)
CALL SYMPOI (1.75,0.,.15,ELAR,0.,42)
CALL PLOT (12.,0.,-3)
100 CONTINUE
RETURN
END

```

+0.30E-2+1.00E+0+1.00E+01